LncRNA *Snhg3* Aggravates Hepatic Steatosis via PPARγ Signaling

Xianghong Xie [1], Mingyue Gao [1], Wei Zhao [1], Chunmei Li [1], Weihong Zhang [2], Jiahui Yang [2], Yinliang Zhang [1], Enhui Chen [3], Yanfang Guo [1], Zeyu Guo [1], Minglong Zhang [3], Ebenezeri Erasto Ngowi [4, 5], Heping Wang [1], Xiaoman Wang [1], Yinghan Zhu [3], Yiting Wang [1], Xiaolu Li [1], Hong Yao [2], Li Yan [3], Fude Fang [1], Meixia Li [6, *], Aijun Qiao [4, 5, *], Xiaojun Liu [1, *]

[1] Department of Biochemistry & Molecular Biology, State Key Laboratory of Common Mechanism Research for Major Diseases, Institute of Basic Medical Sciences Chinese Academy of Medical Sciences & School of Basic Medicine Peking Union Medical College, Beijing 100005, China

[2] Department of Microbiology and Immunology, Shanxi Medical University, Taiyuan 030001, China

[3] Department of Pathophysiology, Institute of Basic Medical Sciences Chinese Academy of Medical Sciences & School of Basic Medicine Peking Union Medical College, Beijing 100005, China

[4] Shanghai Institute of Materia Medica, Chinese Academy of Sciences, 555 Zu Chong Zhi Road, Shanghai 201203, China

[5] Zhongshan Institute for Drug Discovery, Shanghai Institute of Materia Medica, Chinese Academy of Sciences, Zhongshan, Guangdong Province 528400, China

[6] State Key Laboratory of Brain and Cognitive Science, Institute of Biophysics, Chinese Academy of Sciences, Beijing 100101, China

*** Corresponding author**

Meixia Li, Email: limeixia@ibp.ac.cn

State Key Laboratory of Brain and Cognitive Science, Institute of Biophysics,

Chinese Academy of Sciences

#15, Datun Road, Chaoyang District, Beijing 100101, China

Aijun Qiao, Email: qiaoaijun@simm.ac.cn

Zhongshan Institute for Drug Discovery, Shanghai Institute of Materia Medica, Chinese Academy of Sciences

Zhongshan, Guangdong Province 528400, China

& Shanghai Institute of Materia Medica, Chinese Academy of Sciences

555 Zu Chong Zhi Road, Shanghai 201203, China

Xiaojun Liu, Email: xiaojunliu@ibms.pumc.edu.cn

State Key Laboratory of Common Mechanism Research for Major Diseases, Institute of Basic Medical Sciences Chinese Academy of Medical Sciences & School of Basic Medicine Peking Union Medical College

#5 Dongdan santiao, Beijing 100005, China

Abstract

LncRNAs are involved in modulating the individual risk and the severity of progression in metabolic dysfunction-associated fatty liver disease (MASLD), but their precise roles remain largely unknown. This study aimed to investigate the role of lncRNA *Snhg3* in the development and progression of MASLD, along with the underlying mechanisms. The result showed that *Snhg3* was significantly downregulated in the liver of high-fat diet-induced obesity (DIO) mice. Notably, palmitic acid promoted the expression of *Snhg3* and overexpression of *Snhg3* increased lipid accumulation in primary hepatocytes. Furthermore, hepatocyte-specific *Snhg3* deficiency decreased body and liver weight, alleviated hepatic steatosis and promoted hepatic fatty acid metabolism in DIO mice, whereas overexpression induced the opposite effect. Mechanistically, *Snhg3* promoted the

expression, stability and nuclear localization of SND1 protein via interacting with SND1, thereby inducing K63-linked ubiquitination modification of SND1. Moreover, *Snhg3* decreased the H3K27me3 level and induced SND1-mediated chromatin loose remodeling, thus reducing H3K27me3 enrichment at the *Pparγ* promoter and enhancing *Pparγ* expression. The administration of PPARγ antagonist T0070907 improved *Snhg3*-aggravated hepatic steatosis. Our study revealed a new signaling pathway, *Snhg3*/SND1/H3K27me3/PPARγ, responsible for MASLD and indicates that lncRNA-mediated epigenetic modification has a crucial role in the pathology of MASLD.

Introduction

Non-alcohol fatty liver disease (NAFLD) is characterized by excess liver fat in the absence of significant alcohol consumption. It can progress from simple steatosis to nonalcoholic steatohepatitis (NASH) and fibrosis and eventually to chronic progressive diseases such as cirrhosis, end-stage liver failure, and hepatocellular carcinoma (Loomba et al., 2021). In 2020, an international panel of experts led a consensus-driven process to develop a more appropriate term for the disease utilizing a 2-stage Delphi consensus, that is, “metabolic dysfunction-associated fatty liver disease (MASLD)” related to systemic metabolic dysregulation (Rinella et al., 2023, Gofton et al., 2023). The pathogenesis of MASLD has not been entirely elucidated. Multifarious factors such as genetic and epigenetic factors, nutritional factors, insulin resistance, lipotoxicity, microbiome, fibrogenesis and hormones secreted from the adipose tissue, are recognized to be involved in the development and progression of MASLD (Buzzetti et al., 2016, Lee et al., 2017, Rada et al., 2020, Sakurai et al., 2021, Friedman et al., 2018). Free fatty acids (FFAs), which are central to the pathogenesis of MASLD, originate from the periphery, mainly via lipolysis of triglyceride in the adipose tissue, or from increased hepatic *de novo* lipogenesis (DNL). Fatty acids in hepatocytes undergo mitochondrial β-oxidation and re-esterification to form triglyceride (TG), which are then exported into the blood as very low-density

lipoproteins or stored in lipid droplets. Hepatic lipotoxicity occurs when the disposal of fatty acids through β-oxidation or the formation of TG is overwhelmed, which leads to endoplasmic reticulum (ER) stress, oxidative stress and inflammasome activation (Friedman et al., 2018). A cluster of differentiation 36/fatty acid translocase (CD36) and cell death-inducing DFF45-like effector proteins A/C (CIDEA/C) are critical for MASLD progression (Matsusue et al., 2008, Koonen et al., 2007, Sans et al., 2019). CD36 can increase FFAs uptake in the liver and drive hepatosteatosis onset. Overexpression of CD36 in hepatocytes increased FFAs uptake and TG storage; conversely, its deletion ameliorated hepatic steatosis and insulin resistance in DIO mice (Rada et al., 2020). Additionally, CIDEA/C can also regulate various aspects of lipid homeostasis, including lipid storage, lipolysis, and lipid secretion (Xu et al., 2024). As a transcription regulator of *Cd36* and *Cidea/c*, peroxisome proliferator-activated receptor γ (PPARγ) plays a crucial role in MASLD progression (Matsusue et al., 2008, Skat-Rordam et al., 2019, Lee et al., 2018, Lee et al., 2023b, Lee et al., 2021, Puri et al., 2008).

Epigenetics, an inheritable phenomenon occurring without altering the DNA sequence, can regulate gene expression through different forms, including DNA methylation, histone modifications, chromatin remodeling, transcriptional control, and non-coding RNAs (Mann, 2014). Histone modifications, including acetylation, methylation, phosphorylation, ubiquitination, ribosylation, and ubiquitin-like protein modification (SUMO), are important epigenetic determinants of chromatin tightness and accessibility (Chen and Pikaard, 1997). Histone methylation is associated with chromatin-specific transcriptional activity states; for example, methylation of lysine 4 of histone H3 (H3K4), H3K36 and H3K79 are linked with a transcriptional activation state, and H3K9, H3K27, and H4K20 with transcriptional repression state (Pirola and Sookoian, 2020). Previous studies have illustrated that epigenetics factors including histone modification play key role in lipid metabolism (Bayoumi et al., 2020, Jun et al., 2012, Byun et al., 2020).

Long non-coding RNAs (lncRNAs) are non-coding RNAs with more than 200 bases in length, can be transcribed by RNA polymerase II, and are comparable to

mRNA but lack the crucial open reading framework required for translation (Ng et al., 2013, Ulitsky and Bartel, 2013). LncRNAs are involved in epigenetic regulation of gene expression at different levels and through different molecular mechanisms such as chromatin remodeling, transcriptional regulation and post-transcriptional processing. Previous studies have indicated that lncRNAs are involved in the pathological progress of MASLD (Bayoumi et al., 2020, Sommerauer and Kutter, 2022). Although histone modification and lncRNAs influence the susceptibility to MASLD, their roles in MASLD remain largely unknown.

Small nucleolar RNA host genes (*Snhgs*), a type of lncRNA, serve as host genes for producing intronic small nucleolar RNAs (snoRNAs) and are mainly related to tumor pathophysiology by regulating proliferation, apoptosis, invasion, and migration (Sen et al., 2020, Zimta et al., 2020). Here, we found that the expression of hepatic *Snhg3* was decreased in high-fat diet (HFD)-induced obesity (DIO) mice. Experiments conducted using *in vivo* and *in vitro* models indicated that *Snhg3* was involved in fatty acid metabolism and hepatic steatosis. Mechanistically, *Snhg3* interacted with staphylococcal nuclease and Tudor domain containing 1 (SND1), a well-understood Tudor protein that participates in lipid metabolism and tumoral behavior by modulating cholesterol and glycerophospholipid metabolism and acylglyceride storage in lipid droplets (Navarro-Imaz et al., 2020). Furthermore, *Snhg3* increased the expression of SND1 by promoting the stability of SND1 mediated by K63-linked ubiquitination and induced nuclear localization of SND1 protein, thereby reducing tri-methylation at H3K27 (H3K27me3) enrichment and boosting chromatin loose remodeling at PPARγ promoter, eventually enhancing *Pparγ*, *Cd36* and *Cidea/c* expressions. Our result indicated that SND1/H3K27me3/PPARγ is partially responsible for *Sngh3*-induced hepatic steatosis.

Results

LncRNA-*Snhg3* is downregulated in DIO mice

Firstly, we analyzed the lncRNAs expression profiles in the livers of DIO mice and normal chow-fed mice (control) by RNA-Seq, and found 18072 hepatic lncRNAs, including 338 differentially expressed lncRNAs (q-value ≤ 0.05, ***Figure 1A and table supplement 1***). Of all *Snhgs*, *Snhg3* had the most prominent expression and exhibited more noticeable downregulation in the liver of the DIO mice compared to the control mice (***Figure 1B***); thus, it was selected for further study. The downregulation of *Snhg3* was confirmed by RT-qPCR (***Figure 1C***). Additionally, the Coding Potential Calculator indicated that *Snhg3* has a coding probability of 0.020757, classifying it as a noncoding sequence (Kang et al., 2017). Localization of *Snhg3* was primarily observed in nuclei with a probability score of 0.451138, as predicted using software prediction (http://lin-group.cn/server/iLoc-LncRNA/predictor.php). The exact nuclear localization of *Snhg3* was further confirmed by nuclear/cytoplasmic fractionation (***Figure 1D***). Interestingly, the expression of *Snhg3* was induced by palmitic acid (PA) in primary hepatocytes (***Figure 1E***). Furthermore, overexpression of *Snhg3* increased lipid accumulation in primary hepatocytes with PA treatment (***Figures 1F and G***).

Hepatocyte-specific *Snhg3* knock-out alleviates hepatic steatosis in DIO mice

Since *Snhg3* was associated with hepatic nutrition change, the role of *Snhg3* was further confirmed by constructing hepatocyte-specific *Snhg3* knock-out (*Snhg3*-HKO) mice (***Figure 2A and Figure 2-figure supplement 1A and B***). The result indicated that body weight was mildly decreased in DIO *Snhg3*-HKO mice compared with the control DIO *Snhg3*-Flox mice (***Figure 2B***). The energy consumption is mainly reflected as the sum of energy utilization during internal heat production using comprehensive laboratory animal monitoring system (CLAMS). Heat production showed an increasing trend but was not statistically significant in DIO *Snhg3*-HKO mice (***Figure 2-figure supplement 1C***). Moreover, there were no obvious differences in total oxygen consumption, carbon dioxide production or respiratory exchange ratio (RER) between DIO *Snhg3*-HKO and control mice (***Figure 2-figure supplement 1C***). Furthermore, insulin sensitivity, not glucose tolerance, was improved in DIO

Snhg3-HKO mice (***Figure 2C***). The DIO *Snhg3*-HKO mice had a decrease in liver weight and the ratio of liver weight/body weight, and improved hepatic steatosis, including decreasing lipid accumulations and the ballooning degeneration of liver cells (***Figures 2D-F***). However, the hepatic fibrosis phenotype showed no difference (***Figure 2-figure supplement 1D***). Serum alanine transaminase (ALT) and aspartate transaminase (AST) levels were significantly decreased in *Snhg3*-HKO mice (***Figure 2G***). Moreover, serum FFAs, TG and TC were also reduced in *Snhg3*-HKO mice (***Figure 2H***). The DIO *Snhg3*-HKO mice exhibited a decrease in inguinal white adipose tissue (iWAT) weight and weight/body weight ratio, while brown adipose (BAT) weight and weight/body weight ratio remained unaltered (***Figure 2-figure supplement 1E***). Additionally, there was no difference in serum insulin between DIO *Snhg3*-HKO mice and control mice (***Figure 2-figure supplement 1F***). These results suggested that hepatic knockout of *Snhg3* improves hepatic steatosis in DIO mice.

Hepatocyte-specific *Snhg3* knock-in aggravates hepatic steatosis in DIO mice

Furthermore, the hepatocyte-specific *Snhg3* knock-in (*Snhg3*-HKI) mice were also constructed to detect the function of *Snhg3* in the liver (***Figure 3A and Figure 3-figure supplement 1A***). The DIO *Snhg3*-HKI mice showed greater weight gains than the control wild type (WT) mice (***Figure 3B***). Insulin sensitivity was also impaired in DIO *Snhg3*-HKI mice (***Figure 3C***). The liver weight and the ratio of liver weight/body weight of DIO *Snhg3*-HKI mice were markedly increased (***Figure 3D***). Also, DIO *Snhg3*-HKI mice exhibited severe hepatic steatosis (***Figures 3E and F***) and higher serum ALT and AST levels (***Figure 3G***). Both serum TC and iWAT weight were increased in DIO *Snhg3*-HKI mice (***Figures 3H and Figure 3-figure supplement 1B***). Similar to DIO *Snhg3*-HKO mice, there was also no differences in heat production, total oxygen consumption, carbon dioxide production, RER, hepatic fibrosis phenotype and serum insulin between DIO *Snhg3*-HKI mice and WT mice (***Figure 3-figure supplement 1C-E***). These findings indicated that upregulation of *Snhg*3 could promote DIO hepatic steatosis.

Snhg3 promotes hepatic steatosis by regulating chromatin remodeling

To clarify the molecular mechanism of *Snhg3* in hepatic steatosis, we investigated the hepatic differentially expressed genes (DEGs) using RNA-Seq. There were 1393 DEGs between the DIO *Snhg3*-HKI and control WT mice, with 1028 genes being upregulated and 365 genes downregulated (log2FC ≥ 1, q-value < 0.001) in the liver of *Snhg3*-HKI mice (***Figure 4A and table supplement 2***). A gene set enrichment analysis (GSEA) of DEGs revealed that *Snhg3* exerts a global effect on the expression of genes involved in fatty acid metabolism and the PPAR signaling pathway (***Figure 4B***). RT-qPCR analysis confirmed that the hepatic expression levels of some genes involved in fatty acid metabolism, including *Cd36*, *Cidea/c*, and stearoyl-CoA desaturase (*Scd1/2*), the key enzymes involved in the biosynthesis of unsaturated fatty acids (Ntambi and Miyazaki, 2003), were upregulated in *Snhg3*-HKO mice and were downregulated in *Snhg3*-HKI mice compared to the controls (***Figure 4C***). LncRNAs in the nucleus can affect gene expression in multiple ways, such as chromatin remodeling, transcriptional regulation, and post-transcriptional processing (Morey and Avner, 2004, Thomson and Dinger, 2016). Since *Snhg3* was mainly localized in the nuclei of hepatocytes, we next checked the genome-wide chromatin accessibility (log2FC > 2, p-value < 0.001) in the liver of DIO *Snhg3*-HKI and WT mice using ATAC-Seq. We discovered that in all 6810 differentially accessible regions (DARs), 4305 (> 63.2%) were more accessible in *Snhg3*-HKI mice and only 2505 (> 36.8%) of peaks were more accessible in control mice (***table supplement 3***), indicating that the chromatin states were 'hyper-accessible' in the liver of *Snhg3*-HKI mice. Moreover, DARs were with relatively few promoter-proximal (Up2k) and exon regions in both the control and *Snhg3*-HKI groups (***Figure 4D***), supporting the idea that gene activation depends on multiple regulatory regions, is not limited to its promoter and exon regions (Ackermann et al., 2016). Furthermore, 3966 genes were associated specifically with the accessible regions in the *Snhg3*-HKI group and only 2451 genes in the WT group (log2FC > 2, p-value < 0.001, ***table supplement 4***). Additionally, *PPARγ* was identified as a potential transcription factor associated with

hyper-accessible regions in the liver of the *Snhg3*-HKI group by HOMER and CREMA (***Figures 4E and F***).

To determine whether open chromatin regions were correlated with gene expression, we integrated ATAC-Seq data (genes associated with DARs, log2FC > 2, p-value < 0.001) with RNA-Seq data (DEGs in DIO *Snhg3*-HKI and control mice, log2FC > 1, q-value < 0.001). Overall, 233 upregulated genes shown in quadrant 2, including *Cd36* and *Cidea/c*, had at least one associated open chromatin region, which accounted for >22.67% (total 1028) of DEGs mapped to ATAC-Seq peaks in the liver of *Snhg3*-HKI mice (***Figures 4G and H, and table supplement 5***). Meanwhile, at least one open chromatin region was associated with 65 downregulated genes in the quadrant 3, which accounted for > 17.81% (total 365) of DEGs mapped to ATAC-Seq peaks in the liver of WT mice (***Figure 4G and table supplement 5***).

Snhg3 induces SND1 expression by interacting with SND1 and enhancing the stability of SND1 protein

To further elucidate the molecular mechanism of *Snhg3* in hepatic steatosis, an RNA pull-down followed by mass spectrometry (MS) assay was performed in primary hepatocytes. The result identified 234 specific *Snhg3*-associated proteins, involved in multiple signaling pathways, including PPAR, NAFLD and fatty acid degradation pathways (***Figures 5A and B, and table supplement 6***). Of these proteins, a well-understood Tudor protein SND1 was also predicted to interact with three fragments of *Snhg3* by bioinformatic method (RBPsuite (sjtu.edu.cn)) (***Figures 5C and D, and table supplement 7***). *Snhg3* coprecipitation with SND1 was confirmed by RNA pull-down coupled with western blotting (***Figure 5E***), which was consistent with the RNA immunoprecipitation (RIP) assay results (***Figure 5F***). Meanwhile, *Snhg3* regulated the protein, not mRNA, expression of SND1 *in vivo* and *in vitro* by mildly promoting the stability of SND1 protein (***Figures 5G-I***). Furthermore, we tested the effect of *Snhg3* on the ubiquitin-modification of SND1 and found that *Snhg3* enhanced SND1 ubiquitination *in vivo* and *in vitro* (***Figures 5K and L***). Previous studies indicated that K48-linked polyubiquitination aids in

proteasome-mediated recognition and degradation and that K63-linked polyubiquitination participates in signaling assemblies and protein stability (Sun et al., 2020). As predicted, *Snhg3* overexpression increased K63-linked ubiquitination modification in endogenous and exogenous SND1 protein, not K48- or K33-linked (***Figures 5M and N***). Additionally, *Snhg3* overexpression enhanced the nuclear localization of SND1 in Hepa1-6 cells with PA treatment (***Figure 5O***). Collectively, these results suggested that *Snhg3* promoted the K63-linked ubiquitination and stability of SND1 protein through interacting with SND1, thus resulting in SND1 protein increase and nuclear localization.

Snhg3 promotes PPARγ expression by decreasing H3K27me3 enrichment at the *Pparγ* promoter

SND1, initially named as p100, is a highly conserved and ubiquitously expressed multifunctional Tudor domain-containing protein that participates in pivotal biological processes like double-stranded RNA editing, pre-mRNA splicing, microRNA-mediating gene silencing and piRNA biogenesis in germlines (Ying and Chen, 2012). Previous studies indicated that Tudor proteins participate in epigenetic regulation by binding to methyl-arginine/lysine residues (Ying and Chen, 2012). However, whether SND1 influences histone modification remains unclear. It is well known that histone modification dynamically regulates specific gene expression by altering the organization and function of chromatin and is involved in the pathophysiology of some diseases, such as histone H3 methylation modification, which may contribute to MASLD pathogenesis (Tessarz and Kouzarides, 2014, Jun et al., 2012, Byun et al., 2020). Considering that H3K27me3, a repressive chromatin mark, plays a role in autophagy-mediated lipid degradation (Byun et al., 2020), we tested the effect of SND1 on H3K27me3. The results revealed that both SND1 and *Snhg3* overexpression reduced the H3K27me3 level (***Figure 6A***). Furthermore, disrupting SND1 expression increased the H3K27me3 level and reversed the *Snhg3*-induced H3K27me3 decrease (***Figures 6B and C***). Moreover, the hepatic H3K27me3 level was upregulated in *Snhg3*-HKO mice but downregulated in

Snhg3-HKI mice (***Figure 6D***). The results indicated that *Snhg3* negatively regulated the H3K27me3 level through SND1.

To further clarify whether *Snhg3*-induced H3K27me3 decrease is involved in hepatic steatosis, we examined the H3K27me3 enrichment in the liver of DIO *Snhg3*-HKO mice using the CUT&Tag assay and detected 10915 peaks (***table supplement 8***). The genomic locations of these peaks were divided into eight categories, and the H3K27me3 signals were predominantly enriched (about 54%) at the 2-kb promoter, 5'-untranslated region (5'-UTR), and exon categories. Meanwhile, very few signals (about 14%) were enriched in the 2-kb downstream and intergenic categories in the liver of DIO *Snhg3*-HKO mice (***Figure 6E***). Moreover, the exon, upstream 2k, 5'-UTR and intron regions of *Pparγ* were enriched with the H3K27me3 mark (fold_enrichment = 4.15697) in the liver of DIO *Snhg3*-HKO mice (***table supplement 8***). Subsequently, ChIP assay revealed that hepatic H3K27me3 enrichment at the *Pparγ* promoter was increased in DIO *Snhg3*-HKO mice but decreased in DIO *Snhg3*-HKI mice (***Figure 6F***). *Snhg3*-overexpression in Hepa1-6 cells yielded similar results (***Figure 6G***).

SND1 mediates *Snhg3*-induced PPARγ upregulation

PPARγ has been reported to influence MASLD progression by regulating target genes such as *Cd36* and *Cidea/c* (Matsusue et al., 2008, Skat-Rordam et al., 2019, Lee et al., 2018, Lee et al., 2023b, Lee et al., 2021). In this study, the mRNA and protein expression levels of hepatic PPARγ were decreased in DIO *Snhg3*-HKO mice and increased in DIO *Snhg3*-HKI mice (***Figures 7A-C***). Additionally, CD36 protein level was decreased in DIO *Snhg3*-HKO mice and increased in DIO *Snhg3*-HKI mice (***Figures 7B and C***). The upregulation of *Snhg3* and SND1 also increased the expression of *Pparγ* and *Cd36 in vitro* (***Figures 7D-F***). Meanwhile, disruption of SND1 expression alleviated *Snhg3*-induced PPARγ increase and lipid accumulation (***Figures 7G-I***). Collectively, these results demonstrated that SND1 mediated *Snhg3*-induced PPARγ and CD36 expression.

PPARγ mediates *Snhg3*-induced hepatic steatosis

Hepatocyte-specific depletion of PPARγ is known to protect mice against NASH and boost the therapeutic efficacy of rosiglitazone, a synthetic PPARγ agonist, in the liver (Lee et al., 2021). Furthermore, PPARγ is an inducer of adipocyte differentiation and a reservoir for excess FFAs, thereby potentially preventing lipotoxicity in other tissues and organs (Medina-Gomez et al., 2007). To this end, we tested the effect of T0070907, a selective PPARγ antagonist, on *Snhg3*-induced hepatic steatosis in DIO mice. The result showed that T0070907 treatment for 8 weeks had no effects on body weight, liver and iWAT weight, and serum FFAs, TG and TC in DIO *Snhg3*-HKI mice, but improved *Snhg3*-induced hepatic steatosis in DIO *Snhg3*-HKI mice (***Figures 8A-D and Figure 8-figure supplement 1***). Moreover, T0070907 mitigated the hepatic *Cd36* and *Cidea/c* increase in DIO *Snhg3*-HKI mice (***Figure 8E***). Additionally, *Snhg3*- and SND1-induced *Cd36* increase also were abolished by T0070907 in hepa1-6 cells (***Figure 8F***). Collectively, these results suggested that PPARγ-mediated *Snhg3*-induced hepatic steatosis.

Discussion

Liver steatosis is common in various metabolic diseases and related disorders, including MASLD. Although lncRNAs are implicated in regulating numerous mechanisms related to liver steatosis and MASLD, their exact function remains to be determined. In this study, lncRNA-*Snhg3* is downregulated in DIO mice and hepatocyte-specific *Snhg3* deficiency improved hepatic steatosis and insulin resistance, while overexpression aggravated hepatic steatosis and insulin resistance in DIO mice. Our results showed that the expression of *Snhg3* was decreased in DIO mice which led us to speculate that the downregulation of *Snhg3* in DIO mice might be a stress protective reaction to high nutritional state, but the specific details need to be clarified. This is probably similar to fibroblast growth factor 21 (FGF21) and growth differentiation factor 15 (GDF15), whose endogenous expression and circulating levels are elevated in obese humans and mice despite their beneficial

effects on obesity and related metabolic complications (Keipert and Ost, 2021). Although FGF21 can be induced by oxidative stress and be activated in obese mice and in NASH patients, elevated FGF21 paradoxically protects against oxidative stress and reduces hepatic steatosis (Tillman and Rolph, 2020).

Excessive hepatic lipid deposition owing to increased FFAs uptake and hepatic DNL impairs autophagy and promotes ER stress and oxidative stress, insulin resistance, inflammation, and liver tissue damage, ultimately aggravating MASLD progression (Rada et al., 2020). In this study, *Snhg3* induced the expression of fatty acid metabolism related genes such as *Cd36*, *Cidea/c* and *Scd1/2*. Under physiological conditions, CD36 expression in hepatocytes was found to be minimal; however, lipid overload or activation of nuclear receptors including PPARα/γ and liver X receptor (LXR), could significantly increase it (Rada et al., 2020). As a transcription regulator of *Cd36* and *Cidea/c*, it is well known that PPARγ plays major adipogenic and lipogenic roles in adipose tissue. Although the expression of PPARγ in the liver is very low under healthy conditions, induced expression of PPARγ in both hepatocytes and non-parenchymal cells (Kupffer cells, immune cells, and hepatic stellate cells (HSCs)) in the liver has a crucial role in the pathophysiology of MASLD (Lee et al., 2023b, Chen et al., 2023, Gross et al., 2017). The activation of PPARγ in the liver induces the adipogenic program to store fatty acids in lipid droplets as observed in adipocytes (Lee et al., 2018). Moreover, the inactivation of liver PPARγ abolished rosiglitazone-induced an increase in hepatic TG and improved hepatic steatosis in lipoatrophic AZIP mice (Gavrilova et al., 2003). Furthermore, there is a strong correlation between the onset of hepatic steatosis and hepatocyte-specific PPARγ expression. Clinical trials have also indicated that increased insulin resistance and hepatic PPARγ expressions were associated with NASH scores in some obese patients (Lee et al., 2023a, Mukherjee et al., 2022). Even though PPARγ's primary function is in adipose tissue, patients with MASLD have much higher hepatic expression levels of PPARγ, reflecting the fact that PPARγ plays different roles in different tissues and cell types (Mukherjee et al., 2022). As these studies mentioned above, our result also hinted at the importance of PPARγ in the pathophysiology of MASLD. *Snhg3*

deficiency or overexpression respectively induced the decrease or increase in hepatic PPARγ. Moreover, administration of PPARγ antagonist T0070907 mitigated the hepatic *Cd36* and *Cidea/c* increase and improved *Snhg3*-induced hepatic steatosis. However, conflicting findings suggest that the expression of hepatic PPARγ is not increased as steatosis develops in humans and in clinical studies and that PPARγ agonists administration didn't aggravate liver steatosis (Gross et al., 2017). Thus, understanding how the hepatic PPARγ expression is regulated may provide a new avenue to prevent and treat the MASLD (Lee et al., 2018).

Hepatotoxicity accelerates the development of progressive inflammation, oxidative stress and fibrosis (Roehlen et al., 2020). Chronic liver injury including MASLD can progress to liver fibrosis with the formation of a fibrous scar. Injured hepatocytes can secrete fibrogenic factors or exosomes containing miRNAs that activate HSCs, the major source of the fibrous scar in liver fibrosis (Kisseleva and Brenner, 2021). Apart from promoting lipogenesis, PPARγ has also a crucial function in improving inflammation and fibrosis (Chen et al., 2023). In this study, no hepatic fibrosis phenotype was seen in *Snhg3*-HKO and *Snhg3*-HKI mice. Moreover, deficiency and overexpression of *Snhg3* respectively decreased and increased the expression of profibrotic genes, such as collagen type I alpha 1/2 (*Col1a1* and *Col1a2*), but had no effects on the pro-inflammatory factors, including transforming growth factor β1 (*Tgfβ1*), tumor necrosis factor α (*Tnfα*), interleukin 6 and 1β (*Il6 and Il1β*) (***figure supplement 1A and B***). Inflammation is an absolute requirement for fibrosis because factors from injured hepatocytes alone are not sufficient to directly activate HSCs and lead to fibrosis (Kisseleva and Brenner, 2021). Additionally, previous studies indicated that exposure to HFD for more 24 weeks causes less severe fibrosis (Alshawsh et al., 2022). In future, the effect of *Snhg3* on hepatic fibrosis in mice need to be elucidated by prolonged high-fat diet feeding or adopting methionine- and choline deficient diet (MCD) feeding.

Epigenetics plays a crucial role in many physiological and pathological situations (Peixoto et al., 2020). Epigenetic regulation induces phenotypic changes that may respond to environmental cues through DNA methylation and histone modification,

chromatin remodeling, and noncoding RNAs (Mann, 2014). Epigenetic changes interact with inherited risk factors to modulate the individual risk of MASLD development and the severity of progression. Epigenetic modifications, including DNA methylation, miRNAs, and histone modifications, have been associated with MASLD (Jonas and Schurmann, 2021, Eslam et al., 2018, Baffy, 2015). To date, there is no approved pharmacologic therapy for MASLD, and the mainstay of management remains lifestyle changes with exercise and dietary modifications (Bayoumi et al., 2020). Therefore, understanding the epigenetic modifications in MASLD pathogenesis might prove a rational strategy to prevent the disease and develop novel therapeutic interventions (Sodum et al., 2021).

LncRNAs, being abundant in the genome participate in regulating the expression of coding genes through various molecular mechanisms, including: (1) transcriptional regulation at the promoter of target genes; (2) inhibiting RNA polymerase II or mediating chromatin remodeling and histone modification; (3) interfering with the splicing and processing of mRNA or producing endogenous siRNA; (4) regulating the activity or cellular localization of the target protein; (5) acting as competitive endogenous RNAs; and (6) riboregulation by forming nucleic acid-protein complex as structural component (Morey and Avner, 2004, Thomson and Dinger, 2016, Sommerauer and Kutter, 2022). However, compared to the large number of lncRNAs, only few have been functionally well-characterized. Collective literature has shown that lncRNAs play a crucial role in MASLD (Sommerauer and Kutter, 2022). This study demonstrated that lncRNA-*Snhg3* participated in the pathology of MASLD by epigenetic modification; that is, *Snhg3* inhibited the H3K27me3 level, and promoted chromatin relaxation at the *Pparγ* promoter and eventually increased PPARγ expression. The results from Ruan et al. demonstrated that more than a third of dynamically expressed lncRNAs were deregulated in a human MASLD cohort and the lncRNA human lncRNA metabolic regulator 1 (hLMR1) positively regulated transcription of genes involved in cholesterol metabolism (Ruan et al., 2021). Previous studies have also demonstrated that several lncRNAs, including FLRL2/3/6/7/8, H19, and MALAT-1, were associated with lipogenesis via proteins in

the PPAR signaling pathway (Mukherjee et al., 2022). Recently, a murine long noncoding single-cell transcriptome analysis elucidated liver lncRNA cell-type specificities, spatial zonation patterns, associated regulatory networks, and temporal patterns of dysregulation during hepatic disease progression. Moreover, a subset of the liver disease-associated regulatory lncRNAs identified have human orthologs (Karri and Waxman, 2023). Based on the aforementioned information, lncRNAs emerge as promising candidates for biomarkers and therapeutic targets for MASLD. *Snhg3* serves as host gene for producing intronic U17 snoRNAs, the H/ACA snoRNA. A previous study found that cholesterol trafficking phenotype was not due to reduced *Snhg3* expression, but rather to haploinsufficiency of U17 snoRNA. Upregulation of hypoxia-upregulated mitochondrial movement regulator (HUMMR) in U17 snoRNA-deficient cells promoted the formation of ER-mitochondrial contacts, resulting in decreasing cholesterol esterification and facilitating cholesterol trafficking to mitochondria (Jinn et al., 2015). Additionally, disruption of U17 snoRNA caused resistance to lipid-induced cell death and general oxidative stress in cultured cells. Furthermore, knockdown of U17 snoRNA *in vivo* protected against hepatic steatosis and lipid-induced oxidative stress and inflammation (Sletten et al., 2021). In this study, the expression of U17 snoRNA decreased in the liver of DIO *Snhg3*-HKO mice and unchanged in the liver of DIO *Snhg3*-HKI mice, but overexpression of U17 snoRNA had no effect on the expression of SND1 and PPARγ (***figure supplement 2A-C***), indicating that *Sngh3* induced hepatic steatosis was independent on U17 snoRNA.

Tudor proteins play vital roles in normal cell viability and growth by diverse epigenetic functions, including methylation dependent chromatin-remodeling, histone-binding, pre-RNA-processing, RNA-silencing, and transposon silencing in ligands (Ying and Chen, 2012). Tudor proteins are divided into four groups: Group1 Tudor proteins bind to methyl-lysine⁄arginine of histone tails, including Tdrd3, PHF1, PHF20, the Jumonji domain-containing protein (JMJD) family and TP53BP1; Group 2 Tudor proteins bind to methyl-arginine of ligands and representative members include SMN and SMNDC1; Group 3 is represented by SND1; and Group 4, contains

many Tudor proteins, including Tdrd1-9 and Tdrd11, that have been identified in methylation-dependent association with PIWI proteins Ago3, Aub and Piwi. In this study, *Snhg3* induced the protein level of SND1 by promoting K63-linked ubiquitination of SND1 and increasing its protein stability. Additionally, *Snhg3*-induced SND1 protein stability seemed subtle, indicating there may be other way for *Snhg3* promotion SND1, such as riboregulation. Some studies suggested that SND1 plays important roles in cancer by interacting with other transcription factors, including PPARγ, signal transducer and activator of transcription 5/6 (STAT6/5) and myeloblastosis oncogene (c-Myb) (Navarro-Imaz et al., 2020, Duan et al., 2014). SND1 could induce adipogenesis and promote the formation of lipid droplets in adipocytes through working as a co-activator of PPARγ and regulating H3 acetylation (Duan et al., 2014). Our study showed that both *Snhg3* and SND1 decreased the H3K27me3 level and promoted the expression of PPARγ. SND1 could interact with *Snhg3* and mediate the *Snhg3*-induced decrease in H3K27me3 and increase in *Pparγ* expression. Furthermore, inhibition of PPARγ with T0070907 alleviated *Snhg3*- and SND1-induced *Cd36* and *Cidea/c* increase and improved *Snhg3*-aggravated hepatic steatosis. In lncRNA riboregulation, the actions of noncoding RNAs mostly rely on interactions with proteins, including canonical or noncanonical RNA-binding proteins (RBPs). Canonical RBPs, such as heterogeneous nuclear ribonucleoproteins (hnRNPs), polypyrimidine tract binding protein 1 (PTBP1) and human antigen R (HUR), are often involved in posttranscriptional regulation, including pre-mRNA processing, RNA stability, RNA decay, or nuclear export (Briata and Gherzi, 2020). Previous studies have demonstrated that some lncRNAs, e.g., LINC01018, MEG3, APOA4-AS, hLMR1, Blnc1 and LncARSR interact with canonical RBPs to govern the progression of MASLD (Sommerauer and Kutter, 2022).

In summary, our study demonstrates that lncRNA-*Snhg3* influenced fatty acid metabolism and aggravated hepatic steatosis under DIO status. Furthermore, *Snhg3* increased the expression, stability, and nuclear localization of SND1 protein by interacting with SND1, thus enhancing the expression of PPARγ via reducing H3K27me3 enrichment and boosting chromatin loose remodeling at the *Pparγ*

promoter, indicating that SND1/H3K27me3/PPARγ is partially responsible for *Snhg3*-induced hepatic steatosis. This study reveals a new signaling pathway, *Snhg3*/SND1/H3K27me3/PPARγ, responsible for hepatic steatosis and provides evidence of lncRNA-mediated epigenetics in the pathophysiology of MASLD (***Figure 8G***).

However, there are still some limitations to this study that require further investigation. Notably, the expression change of H3K27me3, a global repressive histone mark, may affect multiple downstream target genes, including PPARγ; therefore, more target genes involved in MASLD need to be elucidated. Moreover, the precise mechanism by which SND1 regulates H3K27me3 is still unclear and hence requires further investigation. It is crucial to ascertain whether SND1 itself functions as a new demethylase or if it influences other demethylases, such as Jmjd3, enhancer of zeste homolog 2 (EZH2), and ubiquitously transcribed tetratricopeptide repeat on chromosome X (UTX). SND1 has multiple roles through associating with different types of RNA molecules, including mRNA, miRNA, circRNA, dsRNA and lncRNA. SND1 could bind negative-sense SARS-CoV-2 RNA and to promote viral RNA synthesis (Schmidt et al., 2023). SND1 is also involved in hypoxia by negatively regulating hypoxia□related miRNAs (Saarikettu et al., 2023). Furthermore, a recent study revealed that lncRNA SNAI3-AS1 can competitively bind to SND1 and perturb the m6A-dependent recognition of Nrf2 mRNA 3'UTR by SND1, thereby reducing the mRNA stability of Nrf2 (Zheng et al., 2023). Huang et al. also reported that circMETTL9 can directly bind to and increase the expression of SND1 in astrocytes, leading to enhanced neuroinflammation (Huang et al., 2023). However, whether there is an independent-histone methylation role of SND1/lncRNA-*Snhg3* involved in lipid metabolism in the liver needs to be further investigated.

Materials and Methods

Animals and treatments

C57BL/6 *Snhg3*-Flox mice and hepatocyte-specific *Snhg3* knock-in (*Snhg3*-HKI) mice were created using the CRISPR-Cas9 system at Cyagen Biosciences. To engineer the targeting vector for *Snhg3*-Flox mice, the exon 3 of *Snhg3* was selected as the conditional knockout region, and homology arms and the cKO region were generated by PCR using BAC clone as a template. Cas9 and gRNA were co-injected into fertilized eggs with a targeting vector for mice production. The obtained mice were identified by PCR followed by sequence analysis. Hepatocyte-specific *Snhg3* knock-out (*Snhg3*-HKO) mice were generated by crossing *Snhg3*-Flox mice with C57BL/6-Alb-Cre mice. For *Snhg3*-HKI mice, the "Alb promoter-mouse *Snhg3* cDNA-polyA" cassette was inserted into an H11 locus (~0.7 kb 5' of the Eif4enif1 gene and ~4.5 kb 3' of the Drg1 gene), and homology arms were generated by PCR using BAC clone as template to engineer the targeting vector. Cas9 and gRNA were co-injected into fertilized eggs with targeting vector for mice production. The obtained mice were identified by PCR followed by sequence analysis. All mice were housed in the pathogen-free conditions (SPF) facility and maintained on a 12 h light-dark cycle and a regular unrestricted diet. All mice were fed either a normal chow diet (9% fat; Lab Diet) or HFD (60% fat, Research Diets) for inducing obesity and libitum with free access to water. Unless otherwise noted, 6~8-week-old male mice were used for all experiments. 8-week-old mice fed on HFD were injected intraperitoneally (i.p.) with 1mg/kg of T0070907 dissolved in DMSO for 5 days per week for 2 months. Liver tissue samples were analyzed by the High Fatty Sample Total Cholesterol (TC) Content Assay Kit (APPLYGEN, Cat#E1025-105) and the High Fatty Sample Triglyceride (TG) Content Assay Kit (APPLYGEN, Cat#E1026-105), respectively. Serum concentrations of ALT, AST, FFAs, TG and TC were determined using an automated Monarch device (Peking Union Medical College Hospital, Beijing, China). Serum insulin was detected using a mouse insulin ELISA kit (JM-02862M1, Beijing BioDee Biotechnology Co., Ltd.). All animal experiments were conducted under protocols approved by the Animal Research Committee of the Institute of Laboratory Animals, Institute of Basic Medical Sciences

Chinese Academy of Medical Sciences & School of Basic Medicine Peking Union Medical College (ACUC-A01-2022-010).

Cell culture

Primary mouse hepatocytes were isolated from 8-week-old male C57BL/6J mice and cultured in RPMI 1640 medium with 10% FBS as previously described (Matsumoto et al., 2002). Hepa1-6 cells (ATCC, Cat#CRL-1830) were cultured at 37 °C, 5% CO_2 in DMEM (Gibco, Carlsbad, USA) supplemented with 10% FBS, and 1% penicillin-streptomycin. After attachment, the cells were transfected with indicated plasmids or *siSnd1* by Lipofectamine 3000 Transfection Kit (Invitrogen). Cells were treated with and without 0.25 mM PA for 12h - 24h before collection. The sequences of *siSnd1* were seen key resources table.

Plasmid construction

Snhg3 was amplified from liver cDNA and was then constructed into pcDNA3.1 using Kpn I and EcoR I. The primers were seen key resources table.

Real-Time Quantitative PCR (RT-qPCR)

Total RNA was extracted from mouse tissues using a Trizol-based method. Approximately 2 μg of total RNA was reverse-transcribed into a first-strand cDNA pool using reverse transcriptase and random primers, according to the manufacturer's instructions. RT-qPCR was performed using SYBR Green PCR Master Mix (A6002, Promega) with the gene-specific primers (key resources table). All gene expression data were normalized to actin expression levels.

Western blotting

Protein was extracted from frozen tissue samples in cell lysis buffer. In total, protein was loaded onto a 10% SDS-polyacrylamide gel, and separated proteins were transferred to PVDF membranes. Western blot assays were performed using indicated specific antibodies (key resources table). The proteins were quantified by ImageJ software.

Coding potential prediction

The coding potential of *Snhg3* was evaluated by the Coding Potential Calculator at CPC2@CBI,PKU(gao-lab.org) (Kang et al., 2017).

Histopathologic analysis

Liver tissue sections were fixed in 4% paraformaldehyde, then embedded in paraffin and stained with H&E to visualize the general morphological and structural characteristics of tissues. Lipid droplet accumulation in the liver was visualized using Oil red O staining of frozen liver sections that were prepared in optimum cutting temperature (O.C.T.) compound. Liver fibrosis was visualized using Picro Sirius Red Stain.

Subcellular fractionation

A Cytoplasmic & Nuclear fraction Kit (Beyotime Biotechnology, China) was used to detect *Snhg3* expression in cytoplasmic and nuclear fractions. RNA was extracted from the cytoplasmic and nuclear fractions using a Trizol-based method and subjected to qPCR. *Gapdh* was used as a cytoplasmic marker, and *Neat1* and *Xist* were used as a nuclear marker. The percentage of the transcript abundance was calculated using the following formula, Nucleus % = $2^{\wedge Ct(Nucleus)}/(2^{\wedge Ct(Cytoplasm)} + 2^{\wedge Ct(Nucleus)})$, Cytoplasm % = 1- Nucleus %.

Mouse Calorimetry

Male mice were housed individually in metabolic chambers of an Oxymax system (Columbus Instruments). The first readings were taken after a 24-hr acclimation period. Heat production, total carbon dioxide production and oxygen consumption, and RER were determined by Comprehensive laboratory animal monitoring system (CLAMS). The data were analyzed with CalR (calr (calrapp.org)) (Mina et al., 2018).

Insulin Tolerance test (ITT) and Glucose Tolerance test (GTT)

For ITT, male mice fasted for 6 h and received an intraperitoneal injection of human insulin (0.75 IU/kg). For GTT, male mice fasted for 6 h or 16 h received an intraperitoneal injection of glucose (1 g/kg). A series of blood glucose concentrations were measured from tail blood at the indicated times using a One-Touch Ultra® glucometer (LifeScan Inc., Milpitas, CA).

Chromatin Immunoprecipitation (ChIP)

The ChIP assay was performed using Sonication ChIP Kit (Abclonal, Cat#RK20258). Briefly, the liver tissues or primary hepatocytes were collected and cross-linking

fixed. Cross-linked chromatin fragments were precipitated with Rabbit control IgG (Abclonal, Cat#AC005) or anti-H3K27me3 antibody (Abclonal, Cat# A16199) for subsequent PCR analysis using the amplification primers for mouse PPARγ promoter (+101~+420bp) (key resources table).

RNA immunoprecipitation (RIP)

The RIP assay was performed using RIP Assay Kit (BersinBio, Cat#Bes5101). Briefly, Hepa1-6 cells were transfected by indicated plasmids, respectively. The cells were collected, cross-linking fixed and precipitated with Mouse Control IgG (Abclonal, Cat#AC011) or anti-FLAG antibody (Abclonal, Cat#AE005) for subsequent RT-qPCR analysis using the amplification primers for *Snhg3*.

RNA sequencing (RNA-Seq)

The RNA-Seq was performed according to the manufacturer's protocol (BGI-Shenzhen, https://www.yuque.com/yangyulan-ayaeq/oupzan/fuoao4). Briefly, total RNA was extracted from liver of 3 male DIO (27 weeks) mice and 3 male control mice for RNA-Seq to screen the differentially expressed lncRNAs using Trizol (Invitrogen, Carlsbad, CA, USA) according to manual instruction. rRNA in total RNA removed using RNase H kit, was subsequently to construct library and perform sequencing analysis. The data were mapped to mouse genome (GRCm39) by using Bowtie2. The data for the differentially expressed lncRNAs had been deposited to National Genomics Data Center, China National Center for Bioinformation (NGDC-CNCB) (https://ngdc.cncb.ac.cn/) with the dataset identifier CRA009822. Additionally, total RNA was extracted from livers of 3 male DIO *Snhg3*-HKI mice and 3 male DIO WT mice for RNA-Seq to screen the differentially expressed mRNAs using Trizol. Total RNA was enriched by oligo (dT)-attached magnetic beads, followed by library construction and sequencing analysis. The data were mapped to mouse genome (GRCm39) by using Bowtie2. The data for the differentially expressed mRNAs have been deposited to the Sequence Read Archive (SRA) (submit.ncbi.nlm.nih.gov) with the dataset identifier SRR22368163, SRR22368164, SRR22368165, SRR22368166, SRR22368167 and SRR22368168.

Assay for Transposase-Accessible Chromatin with high throughput sequencing (ATAC-Seq)

The ATAC-seq was performed according to manufacturer's protocols (BGI_Shenzhen, https://www.yuque.com/yangyulan-ayaeq/oupzan/lllmzg). Briefly, fresh liver tissue samples from 3 male DIO *Snhg3*-HKI mice and 3 male DIO control mice were flash frozen by liquid nitrogen and then ground completely. The transposition reactions were initiated by adding transposase. The PCR reaction system was configured to initiate PCR amplification of the transposition products. The corresponding library quality control protocol would be selected depending on product requirements. Single-stranded PCR products were produced via denaturation. The reaction system and program for circularization were subsequently configured and set up. Single-stranded cyclized products were produced, while uncyclized linear DNA molecules were digested. Single-stranded circle DNA molecules were replicated via rolling cycle amplification, and a DNA nanoball (DNB) which contain multiple copies of DNA was generated. Sufficient quality DNBs were then loaded into patterned nanoarrays using high-intensity DNA nanochip technique and sequenced through combinatorial Probe-Anchor Synthesis (cPAS). Data were filtered by removing adaptor sequences, contamination and low-quality reads from raw reads. Bowtie2 was used to do genome alignment after evaluating its performance.

Peak Calling was performed by MACS (Model-based Analysis for ChIP-Seq). The candidate Peak region was extended to be long enough for modeling. Dynamic Possion Distribution was used to calculate the p-value of the specific region based on the unique mapped reads. The region would be defined as a Peak when the p-value < 1e-05. MACS works well for the identification of the sharp peaks of most sequence-specific transcription factors.

Peak Distribution On Gene Elements. Peaks were classified based on the location (UCSC annotation data) and showed in the following genome regions: promoter (<=1kb), promoter (1−2kb), promoter (2−3kb), 5'-UTR, 3'-UTR, intergenic, introns, and exons.

Differential Peaks were identified using MAnorm. First, the true intensities of the most common peaks were assumed to be the same between two ATAC-Seq samples. Second, the observed differences in sequence read density in common peaks were presumed to reflect the scaling relationship of ATAC-Seq signals between two samples, which could thus be applied to all peaks. Based on these hypotheses, the log2 ratio of read density between two samples M was plotted against the average log2 read density A for all peaks, and robust linear regression was applied to fit the global dependence between the M-A values of common peaks. Then the derived linear model was used as a reference for normalization and extrapolated to all peaks. Finally, the p-value for each Peak was calculated based on the Bayesian model, the significant regions were picked up if |M=log2FC| > 2 and p-value < 0.001. To identify DARs, the count matrix was input into MAnorm with the cutoff of abs(log2FC)>2 and p-value<0.001. Genomic features of DARs were annotated by R package ChIPseeker (v1.30.3).

Differential motifs analysis. After extracting the corresponding peak sequence, Hypergeometric Optimization of Motif EnRichment (HOMER, Homer Software and Data Download (ucsd.edu)) and Cis-Regulatory Element Motif Activities (CREMA - Cis-Regulatory Element Motif Analysis (unibas.ch)) were used for motif analysis. Genomic regions with differential ATAC peaks were shown using IGV software.

The data of ATAC-seq has been deposited to National Genomics Data Center, China National Center for Bioinformation (NGDC-CNCB) (https://ngdc.cncb.ac.cn/) with the dataset identifier CRA009511.

Integrated analysis ATAC-Seq data with RNA-Seq data

The common number and unique number of genes associated with DARs and DEGs were counted using Wayne comparative analysis. The values of each quadrant satisfying the log2FC condition were selected from DARs-associated genes and DEGs respectively to draw a nine-quadrant plot. Pearson correlation was calculated for both sets of data and p-value was calculated using the Z-test.

Cleavage Under Targets and Tagmentation sequencing (CUT&Tag-Seq)

CUT&Tag was performed according to the Hyperactive Universal CUT&Tag Assay Kit for Illumina (Vazyme, Nanjing, Cat#TD903-01). Briefly, the mixed liver tissues from 3 DIO *Snhg3*-HKO mice were used for the CUT&Tag experiment. pA-Tn5 transposase was used to cut the genome and add a special adaptor sequence to build a library. The single-stranded PCR products were sequenced on illumina/DNBSEQ-T7 platform PE150 (Annoroad Gene Technology Co.Itd). The data were mapped to mouse genome (GRCm38) by using Bowtie2. Genomic features of DARs were annotated by R package ChIPseeker (v1.30.3). The data of Cut&Tag has been deposited to National Genomics Data Center, China National Center for Bioinformation (NGDC-CNCB) (https://ngdc.cncb.ac.cn/) with the dataset identifier CRA009582.

Biotin-RNA pull-down and mass spectrometry assay

Biotin-RNA pull-down assay was performed as described in a previous study(Guo et al., 2018). Briefly, *Snhg3* DNA was amplified from mouse liver cDNA using the primers listed in the Table 1 and lacZ DNA fragment were constructed into pGEM-T easy vector. The pGEM-T-*Snhg3* and pGEM-T-lacZ vectors were linearized by restriction enzyme digestion, then transcribed to *Snhg3* and lacZ fragments. Biotinylated RNAs were transcribed in vitro with Biotin-RNA Labeling Mix (Roche, Indianapolis, IN) and purified with quick spin RNA columns (Roche, Indianapolis, IN). Biotin-labeled RNA or unbiotinylated RNAs was dissolved in RNA structure buffer (10□mM Tris, pH 7.0, 0.1□M KCl, 10□mM MgCl2) to allow formation of the secondary structure. Primary hepatocytes lysates were added to biotin-labeled RNA or unbiotinylated RNA. Streptavidin agarose beads (GE Healthcare, Little Chalfont, UK) were mixed with a pull-down reaction and then rotated constantly. RNA affinity captures were subjected to 12% SDS-PAGE followed by coomassie blue staining or Western blotting. The various bands that were visualized by coomassie blue staining were excised and subjected to mass spectrometry analyses (LC-MS/MS, A TripleTOF ®, ABsciex, Concord, ON). The data of RNA pull-down for *Snhg3*, control or lacZ were deposited to the iProX (https://www.iprox.cn/) with the dataset identifier PXD039526.

Ubiquitination assays

For endogenous ubiquitination assays, Hepa1-6 cells were transfected with the indicated combinations of plasmids, including HA-ubiquitin and *Snhg3* plasmids. For exogenous ubiquitination assays, Hepa1-6 cells were transfected with the indicated combinations of plasmids, including HA-ubiquitin, HA-K33-ubiquitin, HA-K63-ubiquitin, HA-K48-ubiquitin, Flag-SND1 and *Snhg3* plasmids. Cells were treated with 20 μM MG132 proteasome inhibitor (M1902, AbMole) for 6 hours prior to lyse in lysis buffer (200 mM NaCl, 20 mM Tris-HCl (pH 7.4), 2.5 mM MgCl2, 0.5% Triton X-100, 1 mM PMSF, and protease inhibitor cocktail and then were sonicated. After centrifugation at 14,000 g, the cleared lysates were subjected to immunoprecipitation with anti-SND1 antibody (sc-166676, Santa Cruz) for endogenous ubiquitination assays or with anti-DDDDK-tag magnetic beads (M185-10R, MBL) for exogenous ubiquitination assays. The immunocomplexes were collected and subjected to Western blotting with the indicated antibodies.

Statistical analysis

Data analyses were performed with SPSS (Version 17.0, SPSS, Inc.). The curves of body weight and ITT were analyzed using a repeated measure two-way ANOVA. For the other statistical analysis, the Kolmogorov-Smirnov test was firstly used for normality test. For the data conforming to the normal distribution, experiments were analyzed using Independent-Samples T-test or one-way ANOVA. All data were presented as the mean ± SD or the mean ± SEM. * $p < 0.05$ was considered statistically significant.

Acknowledgments

This work was supported by Chinese Academy of Medical Sciences Innovation Fund for Medical Sciences (CIFMS2021-I2M-1-016 to X.L.), National Key R&D Program of China (2022YFC2504002 to L.Y., 2022YFC2504003 to X.L.), Beijing Natural Science Foundation (7242094 to X.L.), the National Natural Science Foundation of China (82270925 to A.Q.), High-level New R&D Institute of Department of Science and Technology of Guangdong Province (2019B090904008 to A.Q.), and High-level

Innovative Research Institute of Department of Science and Technology of Guangdong Province (2021B0909050003 to A.Q.). We thank Dr. Yi Li (Cancer Hospital, Chinese Academy of Medical Sciences and Peking Union Medical College) for providing the plasmid of HA-Ub, HA-Ub-K63 and HA-Ub-K48. We thank Cyagen Biosciences for the collaborative efforts in the creation of *Snhg3*-loxP and liver-specific knock-in *Snhg3* mice. We thank BGI-Shenzhen for the collaborative efforts in RNA-Seq and ATAC-Seq technology. We thank Anoroad gene technology (Beijing) for the collaborative efforts in Cut&Tag-Seq and Jingjie PTM BioLab (Hangzhou) Co. Ltd for the collaborative efforts in mass spectrometry technology resources.

Author Contributions

Xianghong Xie performed all experiments, acquired and analyzed the data, generated the figures and wrote the manuscript. Mingyue Gao, Wei Zhao, Chunmei Li, Weihong Zhang, Jiahui Yang, Yinliang Zhang, Enhui Chen, Yanfang Guo, Zeyu Guo, Minglong Zhang, Yinghan Zhu, Yiting Wang and Xiaolu Li performed experiments, acquired and analyzed the data. Ebenezeri Erasto Ngowi revised the manuscript. Heping Wang and Xiaoman Wang analyzed the data and generated the figures. Hong Yao, Li Yan and Fude Fang provided additional reagents and revised the manuscript. Meixia Li, Aijun Qiao and Xiaojun Liu devised and supervised the experimental plan and edited the manuscript.

Conflicts of Interest

The author(s) declare(s) that there is no conflict of interest regarding the publication of this article.

Data Availability

All data generated and analysed that support the findings of this study are available from the corresponding author upon reasonable request. The lncRNA-Seq data had been deposited to National Genomics Data Center, China National Center for Bioinformation (NGDC-CNCB) (https://ngdc.cncb.ac.cn/) with the dataset identifier CRA009822. The data of RNA pull-down for *Snhg3*, control or lacZ have been

deposited to the iProX (https://www.iprox.cn/) with the dataset identifier PXD039526. The data of RNA-seq have been deposited to the Sequence Read Archive (SRA) with the dataset identifier SRR22368163, SRR22368164, SRR22368165, SRR22368166, SRR22368167 and SRR22368168. The data of ATAC-seq and Cut&Tag have been deposited to National Genomics Data Center, China National Center for Bioinformation (NGDC-CNCB) (https://ngdc.cncb.ac.cn/) with the dataset identifier CRA009511 and CRA009582, respectively.

Supplemental Materials

table supplement 1 - 8.

Supplement data.

References

ACKERMANN, A. M., WANG, Z., SCHUG, J., NAJI, A. & KAESTNER, K. H. 2016. Integration of ATAC-seq and RNA-seq identifies human alpha cell and beta cell signature genes. *Mol Metab,* 5**,** 233-244. DIO:10.1016/j.molmet.2016.01.002, PMID:26977395

ALSHAWSH, M. A., ALSALAHI, A., ALSHEHADE, S. A., SAGHIR, S. A. M., AHMEDA, A. F., AL ZARZOUR, R. H. & MAHMOUD, A. M. 2022. A Comparison of the Gene Expression Profiles of Non-Alcoholic Fatty Liver Disease between Animal Models of a High-Fat Diet and Methionine-Choline-Deficient Diet. *Molecules,* 27. DIO:10.3390/molecules27030858, PMID:35164140

BAFFY, G. 2015. MicroRNAs in Nonalcoholic Fatty Liver Disease. *J Clin Med,* 4**,** 1977-88. DIO:10.3390/jcm4121953, PMID:26690233

BAYOUMI, A., GRONBAEK, H., GEORGE, J. & ESLAM, M. 2020. The Epigenetic Drug Discovery Landscape for Metabolic-associated Fatty Liver Disease. *Trends Genet,* 36**,** 429-441. DIO:10.1016/j.tig.2020.03.003, PMID:32396836

BRIATA, P. & GHERZI, R. 2020. Long Non-Coding RNA-Ribonucleoprotein Networks in the Post-Transcriptional Control of Gene Expression. *Noncoding RNA,* 6. DIO:10.3390/ncrna6030040, PMID:32957640

BUZZETTI, E., PINZANI, M. & TSOCHATZIS, E. A. 2016. The multiple-hit pathogenesis of non-alcoholic fatty liver disease (NAFLD). *Metabolism,* 65**,** 1038-48. DIO:10.1016/j.metabol.2015.12.012, PMID:26823198

BYUN, S., SEOK, S., KIM, Y. C., ZHANG, Y., YAU, P., IWAMORI, N., XU, H. E., MA, J., KEMPER, B. & KEMPER, J. K. 2020. Fasting-induced FGF21 signaling activates hepatic autophagy

and lipid degradation via JMJD3 histone demethylase. *Nat Commun,* 11**,** 807. DIO:10.1038/s41467-020-14384-z, PMID:32042044

CHEN, H., TAN, H., WAN, J., ZENG, Y., WANG, J., WANG, H. & LU, X. 2023. PPAR-gamma signaling in nonalcoholic fatty liver disease: Pathogenesis and therapeutic targets. *Pharmacol Ther,* 245**,** 108391. DIO:10.1016/j.pharmthera.2023.108391, PMID:36963510

CHEN, Z. J. & PIKAARD, C. S. 1997. Epigenetic silencing of RNA polymerase I transcription: a role for DNA methylation and histone modification in nucleolar dominance. *Genes Dev,* 11**,** 2124-36. DIO:10.1101/gad.11.16.2124, PMID:9284051

DUAN, Z., ZHAO, X., FU, X., SU, C., XIN, L., SAARIKETTU, J., YANG, X., YAO, Z., SILVENNOINEN, O., WEI, M. & YANG, J. 2014. Tudor-SN, a novel coactivator of peroxisome proliferator-activated receptor gamma protein, is essential for adipogenesis. *J Biol Chem,* 289**,** 8364-74. DIO:10.1074/jbc.M113.523456, PMID:24523408

ESLAM, M., VALENTI, L. & ROMEO, S. 2018. Genetics and epigenetics of NAFLD and NASH: Clinical impact. *J Hepatol,* 68**,** 268-279. DIO:10.1016/j.jhep.2017.09.003, PMID:29122391

FRIEDMAN, S. L., NEUSCHWANDER-TETRI, B. A., RINELLA, M. & SANYAL, A. J. 2018. Mechanisms of NAFLD development and therapeutic strategies. *Nat Med,* 24**,** 908-922. DIO:10.1038/s41591-018-0104-9, PMID:29967350

GAVRILOVA, O., HALUZIK, M., MATSUSUE, K., CUTSON, J. J., JOHNSON, L., DIETZ, K. R., NICOL, C. J., VINSON, C., GONZALEZ, F. J. & REITMAN, M. L. 2003. Liver peroxisome proliferator-activated receptor gamma contributes to hepatic steatosis, triglyceride clearance, and regulation of body fat mass. *J Biol Chem,* 278**,** 34268-76. DIO:10.1074/jbc.M300043200, PMID:12805374

GOFTON, C., UPENDRAN, Y., ZHENG, M. H. & GEORGE, J. 2023. MAFLD: How is it different from NAFLD? *Clin Mol Hepatol,* 29**,** S17-S31. DIO:10.3350/cmh.2022.0367, PMID:36443926

GROSS, B., PAWLAK, M., LEFEBVRE, P. & STAELS, B. 2017. PPARs in obesity-induced T2DM, dyslipidaemia and NAFLD. *Nat Rev Endocrinol,* 13**,** 36-49. DIO:10.1038/nrendo.2016.135, PMID:27636730

GUO, H., ZHAO, L., SHI, B., BAO, J., ZHENG, D., ZHOU, B. & SHI, J. 2018. GALNT5 uaRNA promotes gastric cancer progression through its interaction with HSP90. *Oncogene,* 37**,** 4505-4517. DIO:10.1038/s41388-018-0266-4, PMID:29743591

HUANG, C., SUN, L., XIAO, C., YOU, W., SUN, L., WANG, S., ZHANG, Z. & LIU, S. 2023. Circular RNA METTL9 contributes to neuroinflammation following traumatic brain injury by complexing with astrocytic SND1. *J Neuroinflammation,* 20**,** 39. DIO:10.1186/s12974-023-02716-x, PMID:36803376

JINN, S., BRANDIS, K. A., REN, A., CHACKO, A., DUDLEY-RUCKER, N., GALE, S. E., SIDHU, R., FUJIWARA, H., JIANG, H., OLSEN, B. N., SCHAFFER, J. E. & ORY, D. S. 2015. snoRNA U17 regulates cellular cholesterol trafficking. *Cell Metab,* 21**,** 855-67. DIO:10.1016/j.cmet.2015.04.010, PMID:25980348

JONAS, W. & SCHURMANN, A. 2021. Genetic and epigenetic factors determining NAFLD risk. *Mol Metab,* 50**,** 101111. DIO:10.1016/j.molmet.2020.101111, PMID:33160101

JUN, H. J., KIM, J., HOANG, M. H. & LEE, S. J. 2012. Hepatic lipid accumulation alters global histone h3 lysine 9 and 4 trimethylation in the peroxisome proliferator-activated receptor alpha network. *PLoS One,* 7**,** e44345. DIO:10.1371/journal.pone.0044345, PMID:22973438

KANG, Y. J., YANG, D. C., KONG, L., HOU, M., MENG, Y. Q., WEI, L. & GAO, G. 2017. CPC2: a fast and accurate coding potential calculator based on sequence intrinsic features. *Nucleic Acids Res,* 45**,** W12-W16. DIO:10.1093/nar/gkx428, PMID:28521017

KARRI, K. & WAXMAN, D. J. 2023. Dysregulation of murine long noncoding single-cell transcriptome in nonalcoholic steatohepatitis and liver fibrosis. *RNA,* 29**,** 977-1006. DIO:10.1261/rna.079580.123, PMID:37015806

KEIPERT, S. & OST, M. 2021. Stress-induced FGF21 and GDF15 in obesity and obesity resistance. *Trends Endocrinol Metab,* 32**,** 904-915. DIO:10.1016/j.tem.2021.08.008, PMID:34526227

KISSELEVA, T. & BRENNER, D. 2021. Molecular and cellular mechanisms of liver fibrosis and its regression. *Nat Rev Gastroenterol Hepatol,* 18**,** 151-166. DIO:10.1038/s41575-020-00372-7, PMID:33128017

KOONEN, D. P., JACOBS, R. L., FEBBRAIO, M., YOUNG, M. E., SOLTYS, C. L., ONG, H., VANCE, D. E. & DYCK, J. R. 2007. Increased hepatic CD36 expression contributes to dyslipidemia associated with diet-induced obesity. *Diabetes,* 56**,** 2863-71. DIO:10.2337/db07-0907, PMID:17728375

LEE, J., KIM, Y., FRISO, S. & CHOI, S. W. 2017. Epigenetics in non-alcoholic fatty liver disease. *Mol Aspects Med,* 54**,** 78-88. DIO:10.1016/j.mam.2016.11.008, PMID:27889327

LEE, S. M., MURATALLA, J., KARIMI, S., DIAZ-RUIZ, A., FRUTOS, M. D., GUZMAN, G., RAMOS-MOLINA, B. & CORDOBA-CHACON, J. 2023a. Hepatocyte PPARgamma contributes to the progression of non-alcoholic steatohepatitis in male and female obese mice. *Cell Mol Life Sci,* 80**,** 39. DIO:10.1007/s00018-022-04629-z, PMID:36629912

LEE, S. M., MURATALLA, J., SIERRA-CRUZ, M. & CORDOBA-CHACON, J. 2023b. Role of hepatic peroxisome proliferator-activated receptor gamma in non-alcoholic fatty liver disease. *J Endocrinol,* 257. DIO:10.1530/JOE-22-0155, PMID:36688873

LEE, S. M., PUSEC, C. M., NORRIS, G. H., DE JESUS, A., DIAZ-RUIZ, A., MURATALLA, J., SARMENTO-CABRAL, A., GUZMAN, G., LAYDEN, B. T. & CORDOBA-CHACON, J. 2021. Hepatocyte-Specific Loss of PPARgamma Protects Mice From NASH and Increases the Therapeutic Effects of Rosiglitazone in the Liver. *Cell Mol Gastroenterol Hepatol,* 11**,** 1291-1311. DIO:10.1016/j.jcmgh.2021.01.003, PMID:33444819

LEE, Y. K., PARK, J. E., LEE, M. & HARDWICK, J. P. 2018. Hepatic lipid homeostasis by peroxisome proliferator-activated receptor gamma 2. *Liver Res,* 2**,** 209-215. DIO:10.1016/j.livres.2018.12.001, PMID:31245168

LOOMBA, R., FRIEDMAN, S. L. & SHULMAN, G. I. 2021. Mechanisms and disease consequences of nonalcoholic fatty liver disease. *Cell,* 184**,** 2537-2564. DIO:10.1016/j.cell.2021.04.015, PMID:33989548

MANN, D. A. 2014. Epigenetics in liver disease. *Hepatology,* 60**,** 1418-25. DIO:10.1002/hep.27131, PMID:24633972

MATSUMOTO, M., OGAWA, W., TESHIGAWARA, K., INOUE, H., MIYAKE, K., SAKAUE, H. & KASUGA, M. 2002. Role of the insulin receptor substrate 1 and phosphatidylinositol 3-kinase signaling pathway in insulin-induced expression of sterol regulatory element binding protein 1c and glucokinase genes in rat hepatocytes. *Diabetes,* 51**,** 1672-80. PMID:12031952

MATSUSUE, K., KUSAKABE, T., NOGUCHI, T., TAKIGUCHI, S., SUZUKI, T., YAMANO, S. & GONZALEZ, F. J. 2008. Hepatic steatosis in leptin-deficient mice is promoted by the PPARgamma target gene Fsp27. *Cell Metab,* 7**,** 302-11. DIO:10.1016/j.cmet.2008.03.003, PMID:18396136

MEDINA-GOMEZ, G., GRAY, S. L., YETUKURI, L., SHIMOMURA, K., VIRTUE, S., CAMPBELL, M., CURTIS, R. K., JIMENEZ-LINAN, M., BLOUNT, M., YEO, G. S., LOPEZ, M., SEPPANEN-LAAKSO, T., ASHCROFT, F. M., ORESIC, M. & VIDAL-PUIG, A. 2007. PPAR gamma 2 prevents lipotoxicity by controlling adipose tissue expandability and peripheral lipid metabolism. *PLoS Genet,* 3**,** e64. DIO:10.1371/journal.pgen.0030064, PMID:17465682

MINA, A. I., LECLAIR, R. A., LECLAIR, K. B., COHEN, D. E., LANTIER, L. & BANKS, A. S. 2018. CalR: A Web-Based Analysis Tool for Indirect Calorimetry Experiments. *Cell Metab,* 28**,** 656-666 e1. DIO:10.1016/j.cmet.2018.06.019, PMID:30017358

MOREY, C. & AVNER, P. 2004. Employment opportunities for non-coding RNAs. *FEBS Lett,* 567**,** 27-34. DIO:10.1016/j.febslet.2004.03.117, PMID:15165889

MUKHERJEE, A. G., WANJARI, U. R., GOPALAKRISHNAN, A. V., KATTURAJAN, R., KANNAMPUZHA, S., MURALI, R., NAMACHIVAYAM, A., GANESAN, R., RENU, K., DEY, A., VELLINGIRI, B. & PRINCE, S. E. 2022. Exploring the Regulatory Role of ncRNA in NAFLD: A Particular Focus on PPARs. *Cells,* 11. DIO:10.3390/cells11243959, PMID:36552725

NAVARRO-IMAZ, H., OCHOA, B., GARCIA-ARCOS, I., MARTINEZ, M. J., CHICO, Y., FRESNEDO, O. & RUEDA, Y. 2020. Molecular and cellular insights into the role of SND1 in lipid metabolism. *Biochim Biophys Acta Mol Cell Biol Lipids,* 1865**,** 158589. DIO:10.1016/j.bbalip.2019.158589, PMID:31978555

NG, S. Y., LIN, L., SOH, B. S. & STANTON, L. W. 2013. Long noncoding RNAs in development and disease of the central nervous system. *Trends Genet,* 29**,** 461-8. DIO:10.1016/j.tig.2013.03.002, PMID:23562612

NTAMBI, J. M. & MIYAZAKI, M. 2003. Recent insights into stearoyl-CoA desaturase-1. *Curr Opin Lipidol,* 14**,** 255-61. DIO:10.1097/00041433-200306000-00005, PMID:12840656

PEIXOTO, P., CARTRON, P. F., SERANDOUR, A. A. & HERVOUET, E. 2020. From 1957 to Nowadays: A Brief History of Epigenetics. *Int J Mol Sci,* 21. DIO:10.3390/ijms21207571, PMID:33066397

PIROLA, C. J. & SOOKOIAN, S. 2020. Epigenetics factors in nonalcoholic fatty liver disease. *Expert Rev Gastroenterol Hepatol***,** 1-16. DIO:10.1080/17474124.2020.1765772, PMID:32476509

PURI, V., RANJIT, S., KONDA, S., NICOLORO, S. M., STRAUBHAAR, J., CHAWLA, A., CHOUINARD, M., LIN, C., BURKART, A., CORVERA, S., PERUGINI, R. A. & CZECH, M. P. 2008. Cidea is associated with lipid droplets and insulin sensitivity in humans. *Proc Natl Acad Sci U S A,* 105**,** 7833-8. DIO:10.1073/pnas.0802063105, PMID:18509062

RADA, P., GONZALEZ-RODRIGUEZ, A., GARCIA-MONZON, C. & VALVERDE, A. M. 2020. Understanding lipotoxicity in NAFLD pathogenesis: is CD36 a key driver? *Cell Death Dis,* 11**,** 802. DIO:10.1038/s41419-020-03003-w, PMID:32978374

RINELLA, M. E., LAZARUS, J. V., RATZIU, V., FRANCQUE, S. M., SANYAL, A. J., KANWAL, F., ROMERO, D., ABDELMALEK, M. F., ANSTEE, Q. M., ARAB, J. P., ARRESE, M., BATALLER, R., BEUERS, U., BOURSIER, J., BUGIANESI, E., BYRNE, C. D., CASTRO NARRO, G. E., CHOWDHURY, A., CORTEZ-PINTO, H., CRYER, D. R., CUSI, K., EL-KASSAS, M., KLEIN, S., ESKRIDGE, W., FAN, J., GAWRIEH, S., GUY, C. D., HARRISON, S. A., KIM, S. U., KOOT, B. G., KORENJAK, M., KOWDLEY, K. V., LACAILLE, F., LOOMBA, R., MITCHELL-THAIN, R., MORGAN, T. R., POWELL, E. E., RODEN, M., ROMERO-GOMEZ, M., SILVA, M., SINGH, S. P., SOOKOIAN, S. C., SPEARMAN, C. W., TINIAKOS, D., VALENTI, L., VOS, M. B., WONG, V. W., XANTHAKOS, S., YILMAZ, Y., YOUNOSSI, Z., HOBBS, A., VILLOTA-RIVAS, M., NEWSOME, P. N. & GROUP, N. N. C. 2023. A multisociety Delphi consensus statement on new fatty liver disease nomenclature. *Hepatology,* 78**,** 1966-1986. DIO:10.1097/HEP.0000000000000520, PMID:37363821

ROEHLEN, N., CROUCHET, E. & BAUMERT, T. F. 2020. Liver Fibrosis: Mechanistic Concepts and Therapeutic Perspectives. *Cells,* 9. DIO:10.3390/cells9040875, PMID:32260126

RUAN, X., LI, P., MA, Y., JIANG, C. F., CHEN, Y., SHI, Y., GUPTA, N., SEIFUDDIN, F., PIROOZNIA, M., OHNISHI, Y., YONEDA, N., NISHIWAKI, M., DUMBOVIC, G., RINN, J. L., HIGUCHI, Y., KAWAI, K., SUEMIZU, H. & CAO, H. 2021. Identification of human long noncoding RNAs associated with nonalcoholic fatty liver disease and metabolic homeostasis. *J Clin Invest,* 131. DIO:10.1172/JCI136336, PMID:33048844

SAARIKETTU, J., LEHMUSVAARA, S., PESU, M., JUNTTILA, I., PARTANEN, J., SIPILA, P., POUTANEN, M., YANG, J., HAIKARAINEN, T. & SILVENNOINEN, O. 2023. The RNA-binding protein Snd1/Tudor-SN regulates hypoxia-responsive gene expression. *FASEB Bioadv,* 5**,** 183-198. DIO:10.1096/fba.2022-00115, PMID:37151849

SAKURAI, Y., KUBOTA, N., YAMAUCHI, T. & KADOWAKI, T. 2021. Role of Insulin Resistance in MAFLD. *Int J Mol Sci,* 22. DIO:10.3390/ijms22084156, PMID:33923817

SANS, A., BONNAFOUS, S., ROUSSEAU, D., PATOURAUX, S., CANIVET, C. M., LECLERE, P. S., TRAN-VAN-NHIEU, J., LUCI, C., BAILLY-MAITRE, B., XU, X., LEE, A. H., MINEHIRA, K., ANTY, R., TRAN, A., IANNELLI, A. & GUAL, P. 2019. The Differential Expression of Cide Family Members is Associated with Nafld Progression from Steatosis to Steatohepatitis. *Sci Rep,* 9**,** 7501. DIO:10.1038/s41598-019-43928-7, PMID:31097771

SCHMIDT, N., GANSKIH, S., WEI, Y., GABEL, A., ZIELINSKI, S., KESHISHIAN, H., LAREAU, C. A., ZIMMERMANN, L., MAKROCZYOVA, J., PEARCE, C., KREY, K., HENNIG, T., STEGMAIER, S., MOYON, L., HORLACHER, M., WERNER, S., AYDIN, J., OLGUIN-NAVA, M., POTABATTULA, R., KIBE, A., DOLKEN, L., SMYTH, R. P., CALISKAN, N., MARSICO, A., KREMPL, C., BODEM, J., PICHLMAIR, A., CARR, S. A., CHLANDA, P., ERHARD, F. & MUNSCHAUER, M. 2023. SND1 binds SARS-CoV-2 negative-sense RNA and promotes viral RNA synthesis through NSP9. *Cell,* 186**,** 4834-4850 e23. DIO:10.1016/j.cell.2023.09.002, PMID:37794589

SEN, R., FALLMANN, J., WALTER, M. & STADLER, P. F. 2020. Are spliced ncRNA host genes distinct classes of lncRNAs? *Theory Biosci,* 139**,** 349-359. DIO:10.1007/s12064-020-00330-6, PMID:33219910

SKAT-RORDAM, J., HOJLAND IPSEN, D., LYKKESFELDT, J. & TVEDEN-NYBORG, P. 2019. A role of peroxisome proliferator-activated receptor gamma in non-alcoholic fatty liver disease. *Basic Clin Pharmacol Toxicol,* 124**,** 528-537. DIO:10.1111/bcpt.13190, PMID:30561132

SLETTEN, A. C., DAVIDSON, J. W., YAGABASAN, B., MOORES, S., SCHWAIGER-HABER, M., FUJIWARA, H., GALE, S., JIANG, X., SIDHU, R., GELMAN, S. J., ZHAO, S., PATTI, G. J., ORY, D. S. & SCHAFFER, J. E. 2021. Loss of SNORA73 reprograms cellular metabolism and protects against steatohepatitis. *Nat Commun,* 12**,** 5214. DIO:10.1038/s41467-021-25457-y, PMID:34471131

SODUM, N., KUMAR, G., BOJJA, S. L., KUMAR, N. & RAO, C. M. 2021. Epigenetics in NAFLD/NASH: Targets and therapy. *Pharmacol Res,* 167**,** 105484. DIO:10.1016/j.phrs.2021.105484, PMID:33771699

SOMMERAUER, C. & KUTTER, C. 2022. Noncoding RNAs and RNA-binding proteins: emerging governors of liver physiology and metabolic diseases. *Am J Physiol Cell Physiol,* 323**,** C1003-C1017. DIO:10.1152/ajpcell.00232.2022, PMID:35968891

SUN, T., LIU, Z. & YANG, Q. 2020. The role of ubiquitination and deubiquitination in cancer metabolism. *Mol Cancer,* 19**,** 146. DIO:10.1186/s12943-020-01262-x, PMID:33004065

TESSARZ, P. & KOUZARIDES, T. 2014. Histone core modifications regulating nucleosome structure and dynamics. *Nat Rev Mol Cell Biol,* 15**,** 703-8. DIO:10.1038/nrm3890, PMID:25315270

THOMSON, D. W. & DINGER, M. E. 2016. Endogenous microRNA sponges: evidence and controversy. *Nat Rev Genet,* 17**,** 272-83. DIO:10.1038/nrg.2016.20, PMID:27040487

TILLMAN, E. J. & ROLPH, T. 2020. FGF21: An Emerging Therapeutic Target for Non-Alcoholic Steatohepatitis and Related Metabolic Diseases. *Front Endocrinol (Lausanne),* 11**,** 601290. DIO:10.3389/fendo.2020.601290, PMID:33381084

ULITSKY, I. & BARTEL, D. P. 2013. lincRNAs: genomics, evolution, and mechanisms. *Cell,* 154**,** 26-46. DIO:10.1016/j.cell.2013.06.020, PMID:23827673

XU, L., LI, L., WU, L., LI, P. & CHEN, F. J. 2024. CIDE proteins and their regulatory mechanisms in lipid droplet fusion and growth. *FEBS Lett*. DIO:10.1002/1873-3468.14823, PMID:38355218

YING, M. & CHEN, D. 2012. Tudor domain-containing proteins of Drosophila melanogaster. *Dev Growth Differ,* 54**,** 32-43. DIO:10.1111/j.1440-169x.2011.01308.x, PMID:23741747

ZHENG, J., ZHANG, Q., ZHAO, Z., QIU, Y., ZHOU, Y., WU, Z., JIANG, C., WANG, X. & JIANG, X. 2023. Epigenetically silenced lncRNA SNAI3-AS1 promotes ferroptosis in glioma via perturbing the m(6)A-dependent recognition of Nrf2 mRNA mediated by SND1. *J Exp Clin Cancer Res,* 42**,** 127. DIO:10.1186/s13046-023-02684-3, PMID:37202791

ZIMTA, A. A., TIGU, A. B., BRAICU, C., STEFAN, C., IONESCU, C. & BERINDAN-NEAGOE, I. 2020. An Emerging Class of Long Non-coding RNA With Oncogenic Role Arises From the

snoRNA Host Genes. *Front Oncol,* 10**,** 389. DIO:10.3389/fonc.2020.00389, PMID:32318335

Figure legends

Figure 1. The expression of hepatic lncRNA-*Snhg3* is downregulated in DIO mice. (**A**) Differentially expressed *lncRNAs* in livers of 6~8-week-old littermate male mice that were fed an HFD and control diet for 27 weeks (n = 3 mice/group). (**B**) Heat map of *Snhgs* in livers of mice as indicated in (**A**) (n = 3 mice/group). (**C**) Expression levels of *Snhg3* in the liver of 6~8-week-old littermate male mice that were fed an HFD and control diet for indicated time period 11, 27 and 40 weeks. (**D**) Relative *Snhg3* expression levels in nuclear and cytosolic fractions of mouse primary hepatocytes. Nuclear controls: *Neat1* and *Xist*; Cytosolic control: *Gapdh*. (**E**) PA promotes the expression of *Snhg3* in primary hepatocytes. (**F** and **G**) Overexpression of *Snhg3* (**F**) induces lipid accumulation (**G**, left, Oil red O staining; right, quantitative analysis) in primary hepatocytes with PA treatment. Data are represented as mean ± SEM. *p < 0.05, **p < 0.01 and ***p < 0.001 by Student's t test.

Figure 2. Hepatocyte-specific *Snhg3* knockout alleviates hepatic steatosis in DIO mice. (**A**) The expression of *Snhg3* was downregulated in the liver of *Snhg3*-HKO mice. *Snhg3*-Flox (n = 6) and *Snhg3*-HKO (n = 5). (**B**) Body weights of DIO *Snhg3*-Flox (n = 6) and *Snhg3*-HKO (n = 5) mice fed HFD for indicated time period. (**C**) ITT (n = 5/group) and GTT (n = 6/group) of DIO *Snhg3*-Flox and *Snhg3*-HKO mice fed HFD for 18 weeks were analyzed, (AUC, Area Under Curve). (**D**) Liver weight (left) and ratio (right) of liver weight/body weight of DIO *Snhg3*-Flox (n = 6) and *Snhg3*-HKO (n = 5) mice fed HFD for 21 weeks. (**E**) H&E and oil red O staining (left) and NASH score (right) of liver of DIO *Snhg3*-Flox and *Snhg3*-HKO mice as indicated in (**D**). Scare bars, 50 μm. (**F**) Hepatic TG and TC contents of mice as indicated in (**D**). (**G**) Serum ALT and AST concentrations of mice as indicated in (**D**).

(**H**) Serum FFAs, TG and TC concentrations of mice as indicated in (**D**). Data are represented as mean ± SEM. *p < 0.05 and **p < 0.01 by two-way ANOVA (**B** and **C**) and by Student's t test (the others).

Figure 3. Hepatocyte-specific *Snhg3* overexpression aggravates hepatic steatosis in DIO mice. (**A**) The expression of *Snhg3* was upregulated in the liver of *Snhg3*-HKI mice. WT (n = 6) and *Snhg3*-HKI (n = 7). (**B**) Body weights of DIO WT mice (n = 6) and *Snhg3*-HKI mice (n = 7) fed HFD for indicated times. (**C**) ITT and GTT of DIO WT (n = 6) and *Snhg3*-HKI (n = 7) mice fed HFD for 11 weeks were analyzed. (**D**) Liver weight (left) and ratio (right) of liver weight/body weight of DIO WT (n = 6) and *Snhg3*-HKI (n = 7) mice fed HFD for 13 weeks. (**E**) Liver H&E and oil red O staining (left) and NASH score (right) of DIO WT and *Snhg3*-HKI mice as indicated in (**D**). Scare bars, 50 μm. (**F**) Hepatic TG and TC contents of mice as indicated in (**D**). (**G**) Serum ALT and AST concentrations of mice as indicated in (**D**). (**H**) Serum FFAs, TG and TG concentrations of mice as indicated in (**D**). Data are represented as mean ± SEM. *p < 0.05, **p < 0.01 and ***p < 0.001 by two-way ANOVA (**B** and **C**) and by Student's t test (the others).

Figure 4. *Snhg3* promotes hepatic steatosis through regulating chromatin remodeling. (**A**) Differentially expressed genes in livers of DIO *Snhg3*-HKI and WT mice (n = 3 mice/group). (**B**) GSEA showing the enrichment of PPAR signaling pathway (up) and fatty acid metabolism (down) (KEGG pathway database) in livers of DIO *Snhg3*-HKI and WT mice (n = 3 mice/group). (**C**) Relative hepatic mRNA levels of fatty acid metabolism were measured in DIO *Snhg3*-HKO (up) mice and DIO *Snhg3*-HKI mice (down) compared to the controls. (**D**) Genome distribution ratio of the differentially accessible regions in the liver between DIO WT and DIO *Snhg3*-HKI mice by ATAC-Seq. (**E** and **F**) The transcription factors analysis in the accessible regions of the liver of DIO *Snhg3*-HKI mice by HOMER (**E**) and CREMA (**F**). (**G**) Integrated ATAC-Seq data with RNA-Seq data of DIO male mice and the control mice. (**H**)

Chromatin accessibility at *Cd36* and *Cidea/c* genes. Data are represented as mean ± SD. *p < 0.05 and **p < 0.01 by Student's t test.

Figure 5. *Snhg3* induces SND1 expression and enhances the stability of SND1 protein through physiologically interacting with SND1. (**A**) Venn diagram of data from RNA pull-down & MS. (**B**) KEGG analysis of genes in specific *Snhg3*-binding proteins from RNA pull-down & MS. (**C**) Venn diagram of data from RNA pull-down & MS and bioinformatics predicted by RBPsuite (sjtu.edu.cn). (**D**) SND1 interacts with different fragments of *Snhg3* predicted by bioinformatics using RBPsuite (sjtu.edu.cn). (**E**) RNA pull-down & Western blotting confirms *Snhg3* interacting with SND1. (**F**) RIP confirms SND1 interacting with *Snhg3*. (**G** and **H**) Relative protein (**G**, up, western blotting; down, quantitative result) and RNA (**H**) levels of *Snd1* were measured in the liver. (**I**) *Snhg3* enhanced the protein level of SND1 in Hepa1-6 cells (up, western blotting; down, quantitative result). (**J**) *Snhg3* promoted the stability of SND1 protein in Hepa1-6 cells (up, western blotting; down, quantitative result). (**K** and **L**) *Snhg3* promoted the ubiquitination of endogenous (**K**) and exogenous (**L**) SND1 protein in Hepa1-6 cells. (**M** and **N**) *Snhg3* increased the K63-linked, not K48-linked and K33-linked, ubiquitination modification of endogenous (**M**) and exogenous (**N**) SND1 protein. (**O**) *Snhg3* induced the nuclear localization of SND1 in Hepa1-6 cells (up, western blotting; down, quantitative result). Data are represented as mean ± SEM. *p < 0.05 and ***p < 0.001 by two-way ANOVA (**J**) or Student's t test (the others).

Figure 6. *Snhg3* increases PPARγ expression through reducing H3K27me3 enrichment at *Pparγ* promoter. (**A**) Overexpression of *Snhg3* or SND1 reduced the H3K27me3 level in Hepa1-6 cells with PA treatment (up, western blotting; down, quantitative result). (**B**) The expression of SND1 was disrupted with siRNA (up, western blotting; down, quantitative result). (**C**) Disruption SND1 expression reversed the *Snhg3*-induced decrease in H3K27me3 in primary hepatocytes (up, western blotting; down, quantitative result). (**D**) The H3K27me3 levels were measured in the

liver of DIO *Snhg3*-HKO and *Snhg3*-HKI mice (up, western blotting; down, quantitative result). (**E**) Genome distribution ratio of H3K27me3 enrichment genetic sequence in the liver of DIO *Snhg3*-HKO mice. (**F** and **G**) ChIP result showed that *Snhg3* affected H3K27me3 enrichment at *Pparγ* promoter *in vivo* (**F**) and *in vitro* (**G**). Data are represented as mean ± SEM. *p < 0.05, **p < 0.01 and ***p < 0.001 by one-way ANOVA (**C**) or by Student's t test (the others).

Figure 7. SND1 mediates *Snhg3*-induced PPARγ upregulation. (**A**) The mRNA levels of *Pparγ* were measured in the liver of DIO *Snhg3*-HKO (left) and *Snhg3*-HKI mice (right). (**B**) The protein level of PPARγ were measured in the liver of DIO *Snhg3*-Flox and *Snhg3*-HKO mice (up, western blotting; down, quantitative result). (**C**) The protein level of PPARγ were measured in the liver of DIO WT and *Snhg3*-HKI mice (up, western blotting; down, quantitative result). (**D** and **E**) Overexpression of *Snhg3* (**D**) and SND1 (**E**) promoted the mRNA expression of *Pparγ* and *Cd36* in primary hepatocytes. (**F**) Overexpression of *Snhg3* and SND1 increased the protein expression of PPARγ in Hepa1-6 cells (up, western blotting; down, quantitative result). (**G**) Disruption SND1 expression alleviated *Snhg3*-induced increase in the protein level of PPARγ in Hepa1-6 cells (left) and mouse primary hepatocytes (MPH, right) with PA treatment (up, western blotting; down, quantitative result). (**H**) Disruption SND1 expression alleviated *Snhg3*-induced increase in the mRNA levels of *Pparγ* and *Cd36* in Hepa1-6 cells with PA treatment. (**I**) Disruption SND1 expression alleviated *Snhg3*-induced increase in lipid accumulation (left, oil red O staining; right, quantitative result) in MPH with PA treatment. Data are represented as mean ± SEM. *p < 0.05, **p < 0.01 and ***p < 0.001 by one-way ANOVA (**G-I**) or by Student's t test (the others).

Figure 8. PPARγ mediates *Snhg3*-induced hepatic steatosis. (**A** and **B**) Body weights (**A**) and liver weight (**B**) of DIO *Snhg3*-HKI mice without (n = 6) or with (n = 7) T0070907 treatment for 8 weeks. (**C**) Serum FFAs, TG and TG concentrations of mice as indicated in (**A**). (**D**) Hepatic H&E and oil red O staining (left) and NASH

score (right) of mice as indicated in *A*. Scare bars, 100 μm. (**E**) T0070907 mitigated the hepatic *Cd36* and *Cidea/c* increase in DIO *Snhg3*-HKI mice. (**F**) T0070907 disrupted *Snhg3*- and SND1-induced *Cd36* increase in Hepa1-6 cells. (**G**) Model of how *Snhg3* and SND1 interacting and influencing chromatin remodeling via H3K27me3, and promoting PPARγ expression thereby resulting in hepatic steatosis. Data are represented as mean ± SEM. *p < 0.05 and ***p < 0.001 by two-way ANOVA (**A**) or by Student's t test for the others.

Figure 2-figure supplement 1. Hepatocyte-specific *Snhg3* knockout improves high-fat diet-induced hepatic steatosis. (**A**) The genome mapping of mouse *Snhg3* (https://www.ncbi.nlm.nih.gov/gene/). (**B**) Schematic diagram for the creation of hepatocyte-specific *Snhg3* knock-out (*Snhg3*-HKO) mice. (**C**) Heat production, total oxygen consumption and carbon dioxide production, and RER of DIO *Snhg3*-Flox (n = 6) and *Snhg3*-HKO (n = 6) mice fed HFD for 16 weeks were measured by CLAMS. (**D**) Liver fibrosis DIO *Snhg3*-Flox and *Snhg3*-HKO mice fed HFD for 16 weeks was visualized using Picro Sirius Red Stain. Scare bars, 50 μm. (**E**) iWAT weight (left) and ratio (right) of iWAT weight/body weight of mice as indicated in DIO *Snhg3*-Flox (n = 6) and *Snhg3*-HKO (n = 5) mice fed HFD. (**F**) Serum insulin concentration of mice as indicated in DIO *Snhg3*-Flox (n = 6) and *Snhg3*-HKO (n = 5) mice fed HFD. Data are represented as mean ± SEM. ***p < 0.001 by Student's t test (the others).

Figure 3-figure supplement 1. Hepatocyte-specific *Snhg3* overexpression aggravates high-fat diet-induced hepatic steatosis. (**A**) Schematic diagram for the creation of hepatocyte-specific *Snhg3* knock-in (*Snhg3*-HKI) mice. (**B**) iWAT weight (left) and ratio (right) of iWAT weight/body weight of mice as indicated in DIO WT (n = 6) and *Snhg3*-HKI (n = 7) mice fed HFD for 9 weeks. (**C**) Heat production, total oxygen consumption and carbon dioxide production, and RER of DIO WT (n = 4) and *Snhg3*-HKI (n = 4) mice fed HFD for 9 weeks were measured by CLAMS. (**D**) Liver fibrosis in DIO WT and *Snhg3*-HKI mice fed HFD for 9 weeks was visualized using

Picro Sirius Red Stain. Scare bars, 50 μm. (**E**) Serum insulin concentration of mice as indicated in DIO WT (n = 6) and *Snhg3*-HKI (n = 7) mice fed HFD for 9 weeks. Data are represented as mean ± SEM. ***p < 0.001 by Student's t test (the others).

Figure 8-figure supplement 1. Fat weight of DIO *Snhg3*-HKI mice without (n = 6) or with (n = 7) T0070907 treatment for 8 weeks. Data are represented as mean ± SEM.

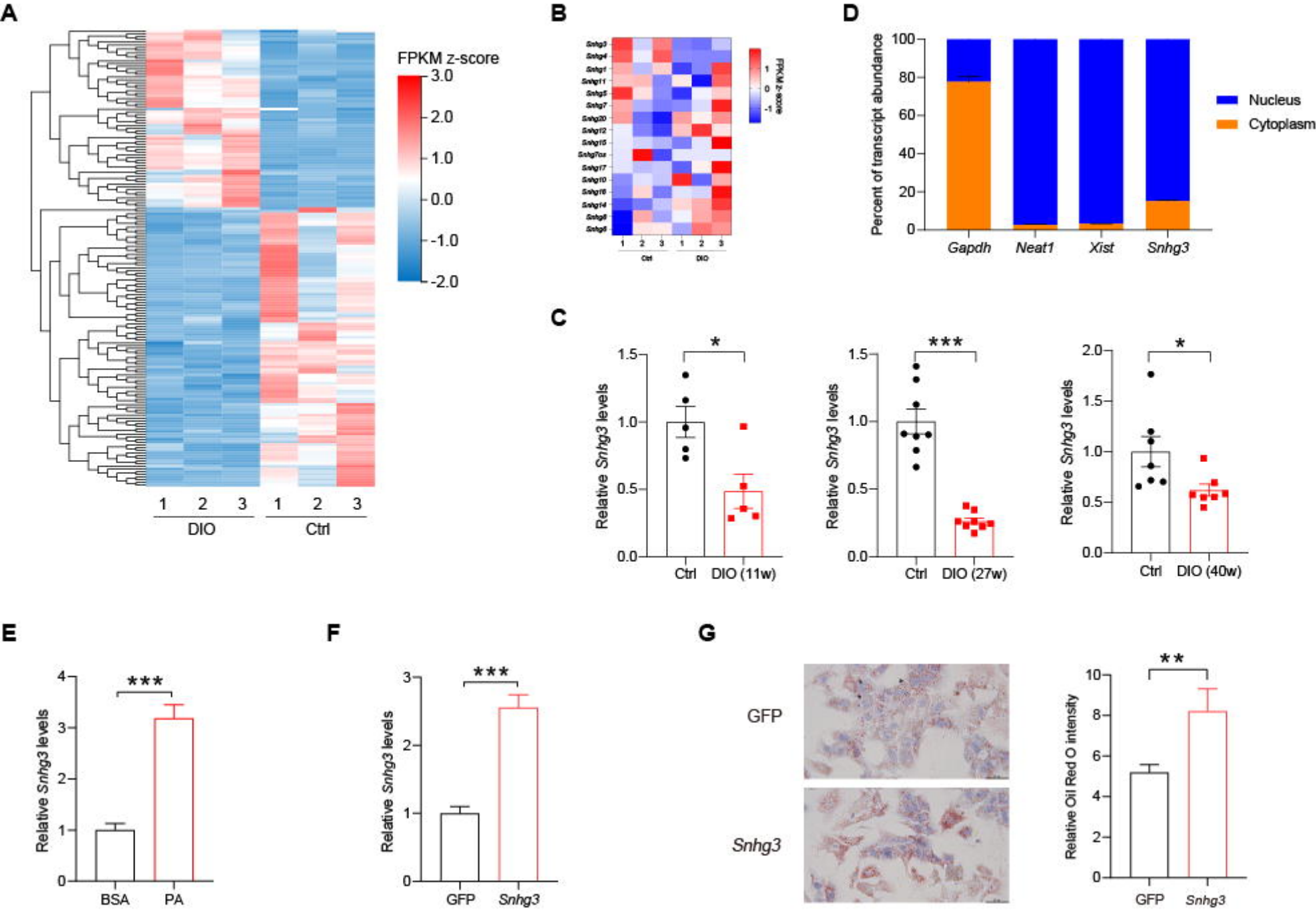
A
FPKM z-score
3.0
2.0
1.0
0.0
-1.0
-2.0
1 2 3 1 2 3
DIO
Ctrl
B
FPKM z-score
1 2 3 1 2 3
Ctrl
DIO
D
Percent of transcript abundance
100
80
60
40
20
0
Gapdh
Neat1
Xist
Snhg3
Nucleus
Cytoplasm
C
Relative Snhg3 levels
*
Ctrl
DIO (11w)
***
Ctrl
DIO (27w)
*
Ctrl
DIO (40w)
E
Relative Snhg3 levels
***
BSA
PA
F
Relative Snhg3 levels
***
GFP
Snhg3
G
GFP
Snhg3
Relative Oil Red O intensity
**
GFP
Snhg3

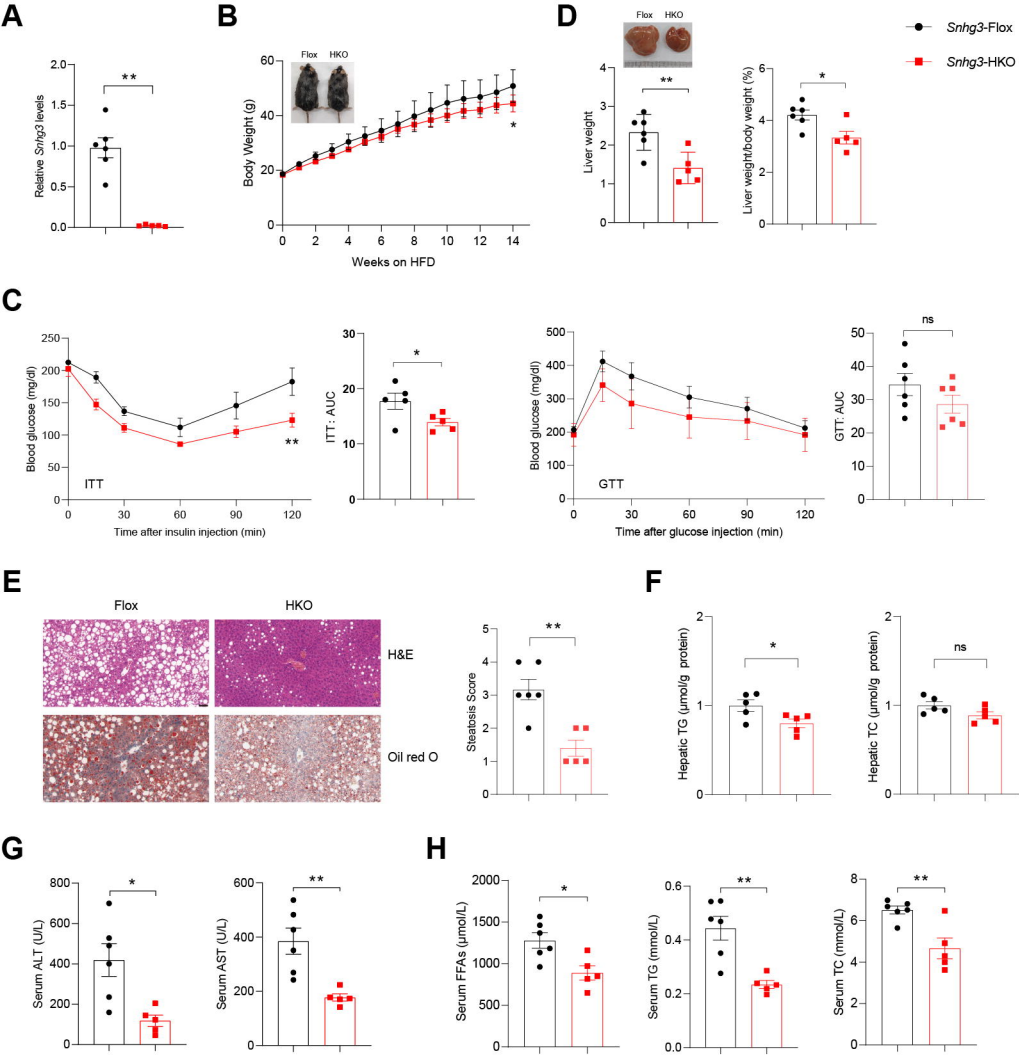
A
Relative Snhg3 levels
**
B
Flox
HKO
Body Weight (g)
Weeks on HFD
*
D
Flox
HKO
Snhg3-Flox
Snhg3-HKO
Liver weight
**
Liver weight/body weight (%)
*
C
Blood glucose (mg/dl)
ITT
Time after insulin injection (min)
**
ITT : AUC
*
Blood glucose (mg/dl)
GTT
Time after glucose injection (min)
GTT: AUC
ns
E
Flox
HKO
H&E
Oil red O
Steatosis Score
**
F
Hepatic TG (μmol/g protein)
*
Hepatic TC (μmol/g protein)
ns
G
Serum ALT (U/L)
*
Serum AST (U/L)
**
H
Serum FFAs (μmol/L)
*
Serum TG (mmol/L)
**
Serum TC (mmol/L)
**

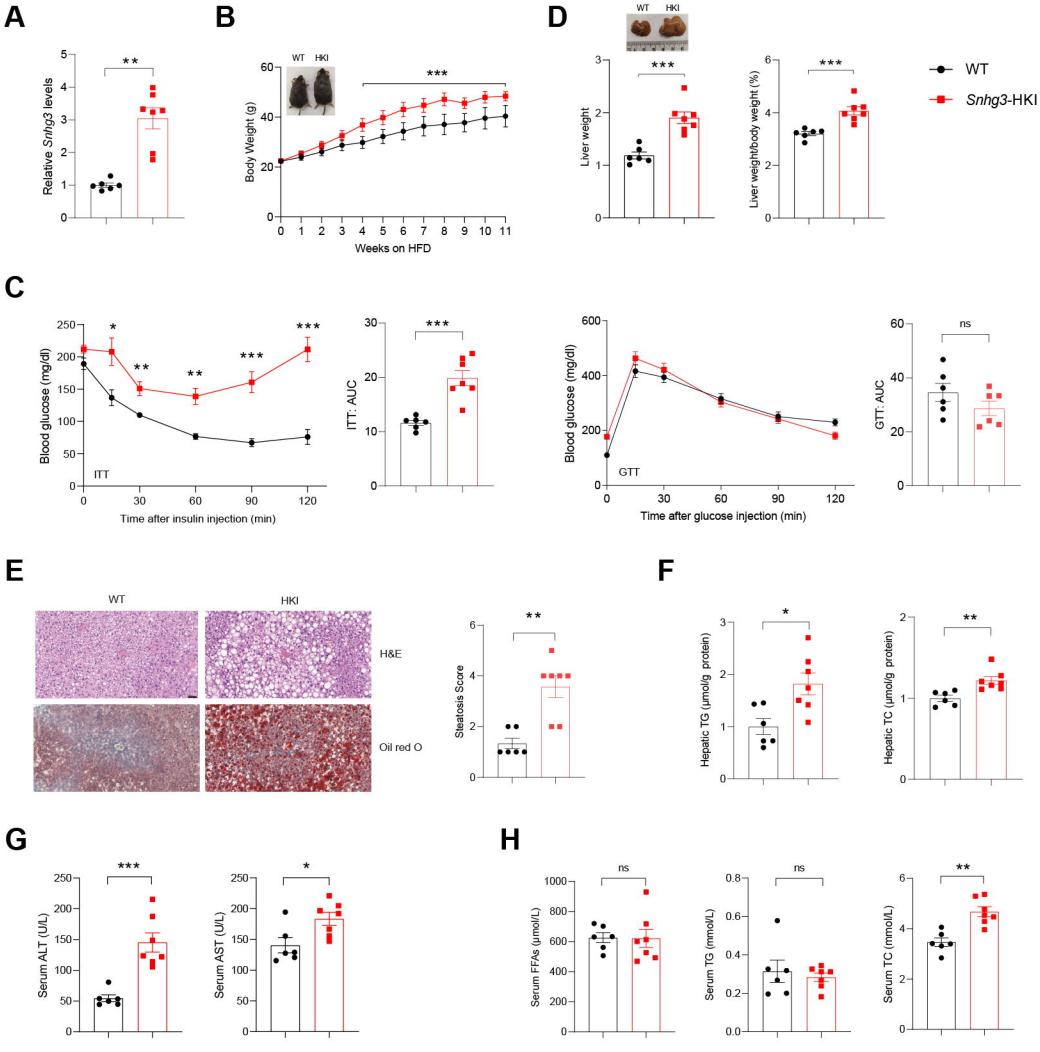
A
Relative Snhg3 levels
**
B
WT
HKI
***
Body Weight (g)
Weeks on HFD
D
WT
HKI
***
Liver weight
***
Liver weight/body weight (%)
WT
Snhg3-HKI
C
Blood glucose (mg/dl)
*
**
**
***
***
ITT
Time after insulin injection (min)
***
ITT: AUC
Blood glucose (mg/dl)
GTT
Time after glucose injection (min)
ns
GTT: AUC
E
WT
HKI
H&E
Oil red O
**
Steatosis Score
F
*
Hepatic TG (μmol/g protein)
**
Hepatic TC (μmol/g protein)
G
***
Serum ALT (U/L)
*
Serum AST (U/L)
H
ns
Serum FFAs (μmol/L)
ns
Serum TG (mmol/L)
**
Serum TC (mmol/L)

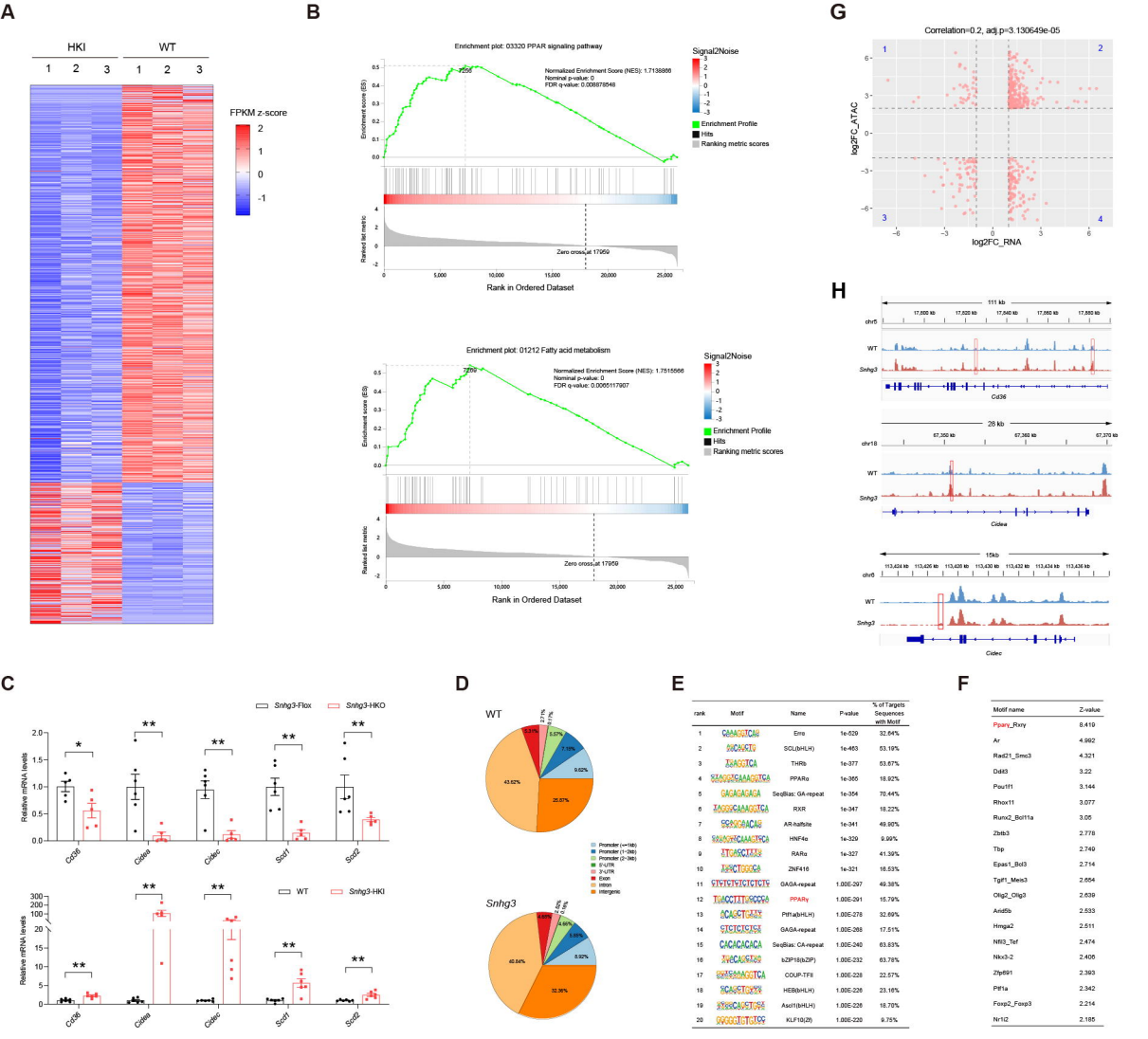
A
HKI
WT
1 2 3 1 2 3
FPKM z-score
2
1
0
-1
B
Enrichment plot: 03320 PPAR signaling pathway
Normalized Enrichment Score (NES): 1.7138866
Nominal p-value: 0
FDR q-value: 0.008878548
7206
Enrichment score (ES)
Signal2Noise
Enrichment Profile
Hits
Ranking metric scores
Ranked list metric
Zero cross at 17959
Rank in Ordered Dataset
Enrichment plot: 01212 Fatty acid metabolism
Normalized Enrichment Score (NES): 1.7515566
Nominal p-value: 0
FDR q-value: 0.0065117907
7206
Zero cross at 17959
Rank in Ordered Dataset
G
Correlation=0.2, adj.p=3.130649e-05
log2FC_ATAC
log2FC_RNA
H
111 kb
chr5
WT
Snhg3
Cd36
26 kb
chr18
Cidea
15kb
chr6
Cidec
C
Snhg3-Flox
Snhg3-HKO
Relative mRNA levels
Cd36
Cidea
Cidec
Scd1
Scd2
WT
Snhg3-HKI
D
WT
Snhg3
Promoter (<=1kb)
Promoter (1~2kb)
Promoter (2~3kb)
5'-UTR
3'-UTR
Exon
Intron
Intergenic
E
rank
Motif
Name
P-value
% of Targets Sequences with Motif
1 Erra 1e-529 32.64%
2 SCL(bHLH) 1e-463 53.19%
3 THRb 1e-377 53.67%
4 PPARa 1e-365 18.92%
5 SeqBias: GA-repeat 1e-354 70.44%
6 RXR 1e-347 18.22%
7 AR-halfsite 1e-341 49.90%
8 HNF4a 1e-329 9.99%
9 RARa 1e-327 41.39%
10 ZNF416 1e-321 16.53%
11 GAGA-repeat 1.00E-297 49.38%
12 PPARγ 1.00E-291 15.79%
13 Ptf1a(bHLH) 1.00E-278 32.69%
14 GAGA-repeat 1.00E-268 17.51%
15 SeqBias: CA-repeat 1.00E-240 63.63%
16 bZIP18(bZIP) 1.00E-232 63.78%
17 COUP-TFII 1.00E-228 22.57%
18 HEB(bHLH) 1.00E-226 23.16%
19 Ascl1(bHLH) 1.00E-226 18.70%
20 KLF10(Zf) 1.00E-220 9.75%
F
Motif name
Z-value
Pparγ_Rxrγ 8.419
Ar 4.992
Rad21_Smc3 4.321
Ddit3 3.22
Pou1f1 3.144
Rhox11 3.077
Runx2_Bcl11a 3.05
Zbtb3 2.778
Tbp 2.749
Epas1_Bcl3 2.714
Tgif1_Meis3 2.654
Olig2_Olig3 2.639
Arid5b 2.533
Hmga2 2.511
Nfil3_Tef 2.474
Nkx3-2 2.406
Zfp691 2.393
Ptf1a 2.342
Foxp2_Foxp3 2.214
Nr1i2 2.185

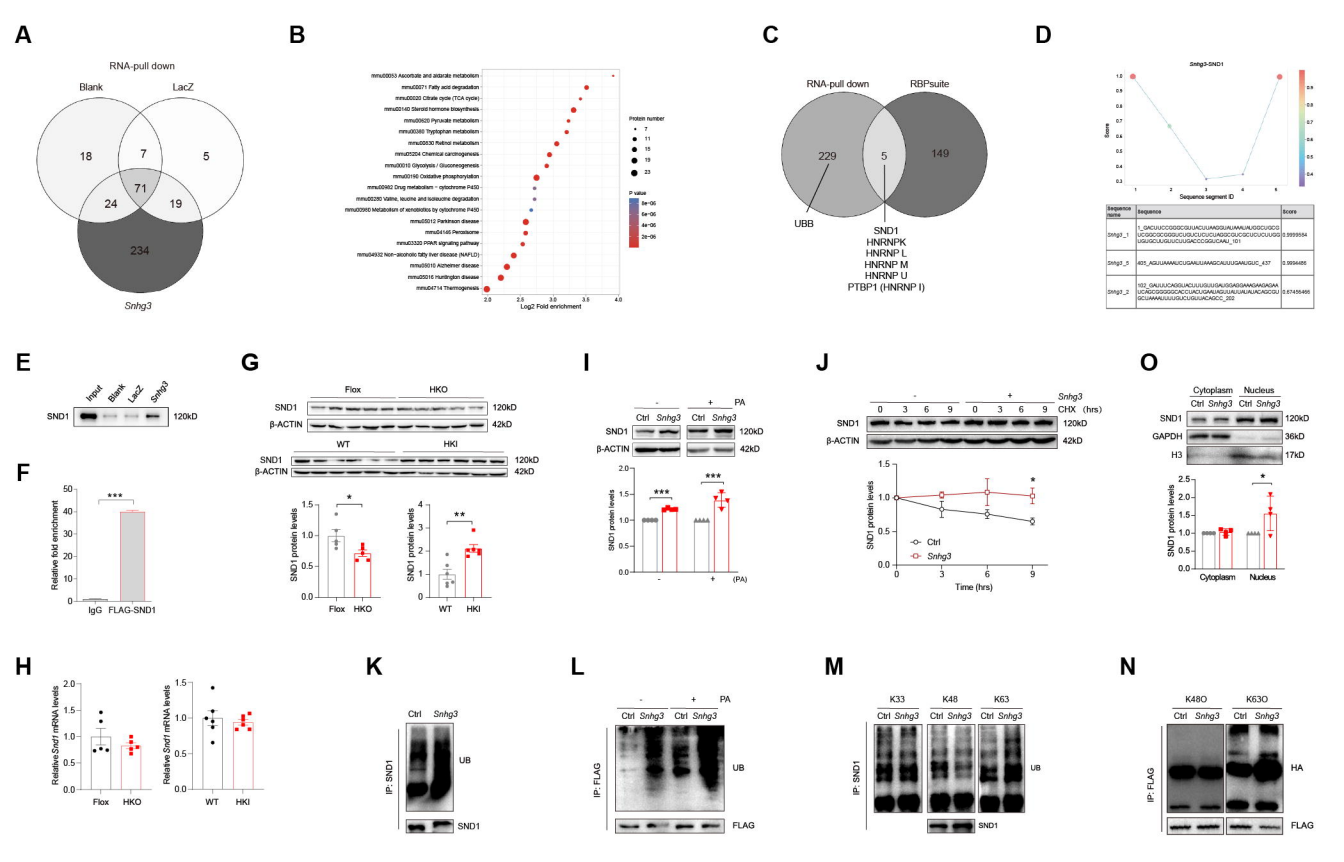
A
RNA-pull down
Blank
LacZ
18
7
5
71
24
19
234
Snhg3
B
mmu00053 Ascorbate and aldarate metabolism
mmu00071 Fatty acid degradation
mmu00020 Citrate cycle (TCA cycle)
mmu00140 Steroid hormone biosynthesis
mmu00620 Pyruvate metabolism
mmu00380 Tryptophan metabolism
mmu00830 Retinol metabolism
mmu05204 Chemical carcinogenesis
mmu00010 Glycolysis / Gluconeogenesis
mmu00190 Oxidative phosphorylation
mmu00982 Drug metabolism - cytochrome P450
mmu00280 Valine, leucine and isoleucine degradation
mmu00980 Metabolism of xenobiotics by cytochrome P450
mmu05012 Parkinson disease
mmu04146 Peroxisome
mmu03320 PPAR signaling pathway
mmu04932 Non-alcoholic fatty liver disease (NAFLD)
mmu05010 Alzheimer disease
mmu05016 Huntington disease
mmu04714 Thermogenesis
2.0
2.5
3.0
3.5
4.0
Log2 Fold enrichment
Protein number
7
11
15
19
23
P value
8e-06
6e-06
4e-06
2e-06
C
RNA-pull down
RBPsuite
229
5
149
UBB
SND1
HNRNPK
HNRNP L
HNRNP M
HNRNP U
PTBP1 (HNRNP I)
D
Snhg3-SND1
Score
Sequence segment ID
Sequence name
Sequence
Score
Snhg3_1
1_GACUUCCGGCGUACUUAAGGUAUAAUAUGCCUCCG
UCGGCGCGGGCUCUCUCUAGGCGUCGCUCUCUUGGCG
UGUGCUUGUCCUUGACCCGGUCAAU_101
99999554
Snhg3_5
405_AGUUAAAUCUGAAUUAAGCAUUUGAAUGUC_437
0.9994486
Snhg3_2
102_GAUUUCAGGUUCUUGUUGAUGGAGGAAAGAGAGAA
UCAGCGGGGGCACCUACUGAAUGUUAUAUACAGCGU
GCUAAAUUUUGUCUGUUACAGCC_202
0.67455466
E
Input
Blank
LacZ
Snhg3
SND1
120kD
F
Relative fold enrichment
IgG
FLAG-SND1
G
Flox
HKO
SND1
β-ACTIN
120kD
42kD
WT
HKI
SND1 protein levels
Flox
HKO
WT
HKI
H
Relative Snrf1 mRNA levels
Flox
HKO
WT
HKI
I
PA
Ctrl
Snhg3
SND1 protein levels
(PA)
J
Snhg3
CHX (hrs)
0
3
6
9
SND1
β-ACTIN
120kD
42kD
SND1 protein levels
Ctrl
Snhg3
Time (hrs)
O
Cytoplasm
Nucleus
SND1
GAPDH
H3
120kD
36kD
17kD
SND1 protein levels
K
IP: SND1
UB
SND1
L
PA
IP: FLAG
UB
FLAG
M
K33
K48
K63
IP: SND1
UB
SND1
N
K48O
K63O
IP: FLAG
HA
FLAG

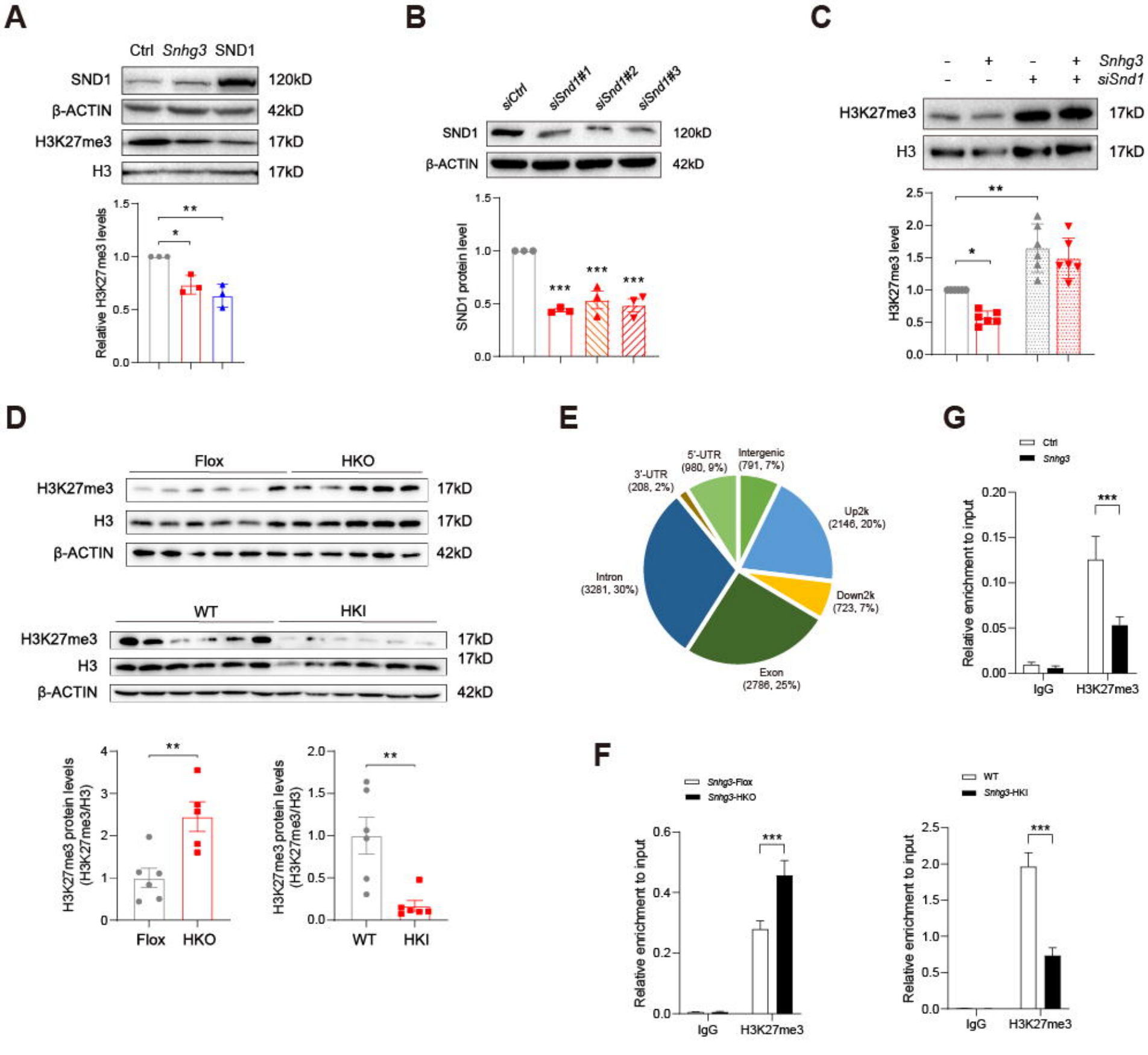
A
Ctrl Snhg3 SND1
SND1
β-ACTIN
H3K27me3
H3
120kD
42kD
17kD
17kD
Relative H3K27me3 levels
B
siCtrl
siSnd1#1
siSnd1#2
siSnd1#3
SND1
β-ACTIN
120kD
42kD
SND1 protein level
C
Snhg3
siSnd1
H3K27me3
H3
17kD
17kD
H3K27me3 level
D
Flox
HKO
WT
HKI
H3K27me3
H3
β-ACTIN
17kD
17kD
42kD
H3K27me3 protein levels (H3K27me3/H3)
E
5'-UTR (980, 9%)
Intergenic (791, 7%)
3'-UTR (208, 2%)
Up2k (2146, 20%)
Intron (3281, 30%)
Down2k (723, 7%)
Exon (2786, 25%)
F
Snhg3-Flox
Snhg3-HKO
WT
Snhg3-HKI
Relative enrichment to input
IgG
H3K27me3
G
Ctrl
Snhg3
Relative enrichment to input
IgG
H3K27me3

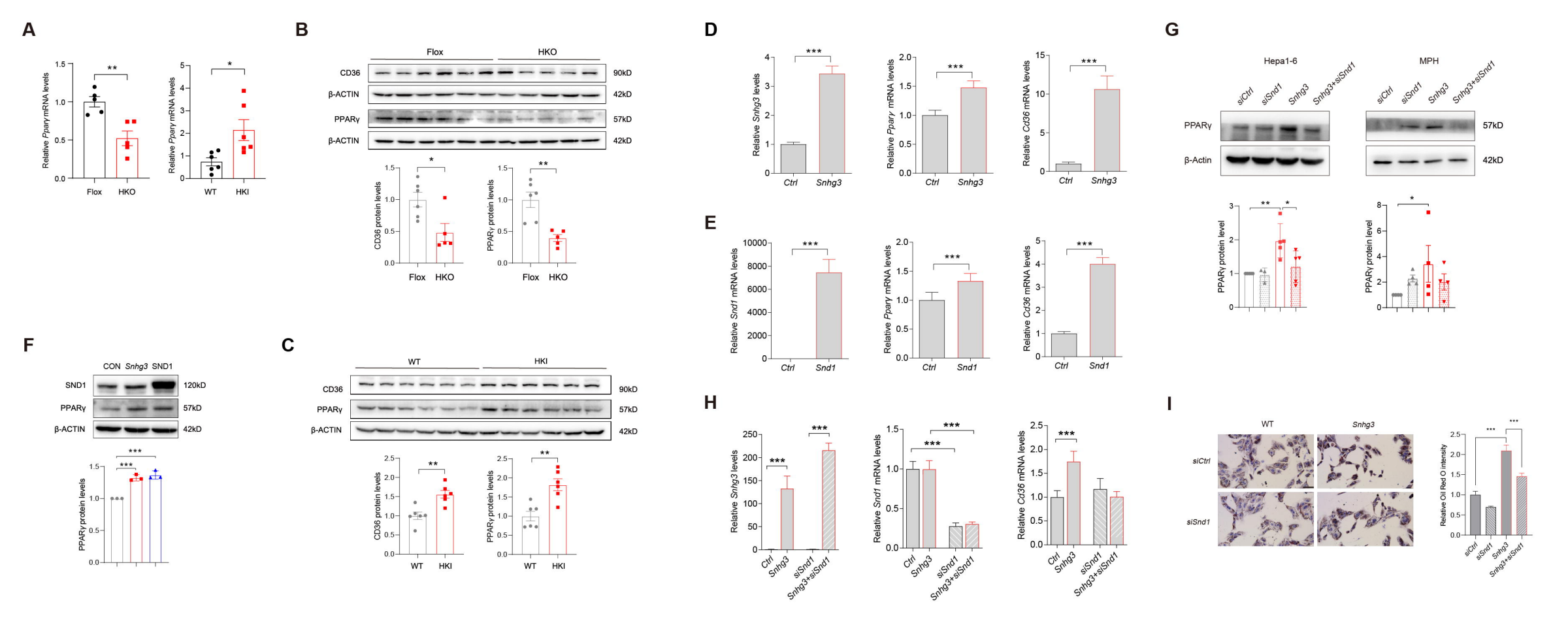
A
Relative Pparγ mRNA levels
Flox
HKO
WT
HKI
B
Flox
HKO
CD36
β-ACTIN
PPARγ
90kD
42kD
57kD
CD36 protein levels
PPARγ protein levels
C
WT
HKI
D
Relative Snhg3 levels
Relative Pparγ mRNA levels
Relative Cd36 mRNA levels
Ctrl
Snhg3
E
Relative Snd1 mRNA levels
Snd1
F
CON
Snhg3
SND1
120kD
PPARγ protein levels
G
Hepa1-6
MPH
siCtrl
siSnd1
Snhg3
Snhg3+siSnd1
PPARγ
β-Actin
PPARγ protein level
H
siSnd1
Snhg3+siSnd1
I
Relative Oil Red O intensity

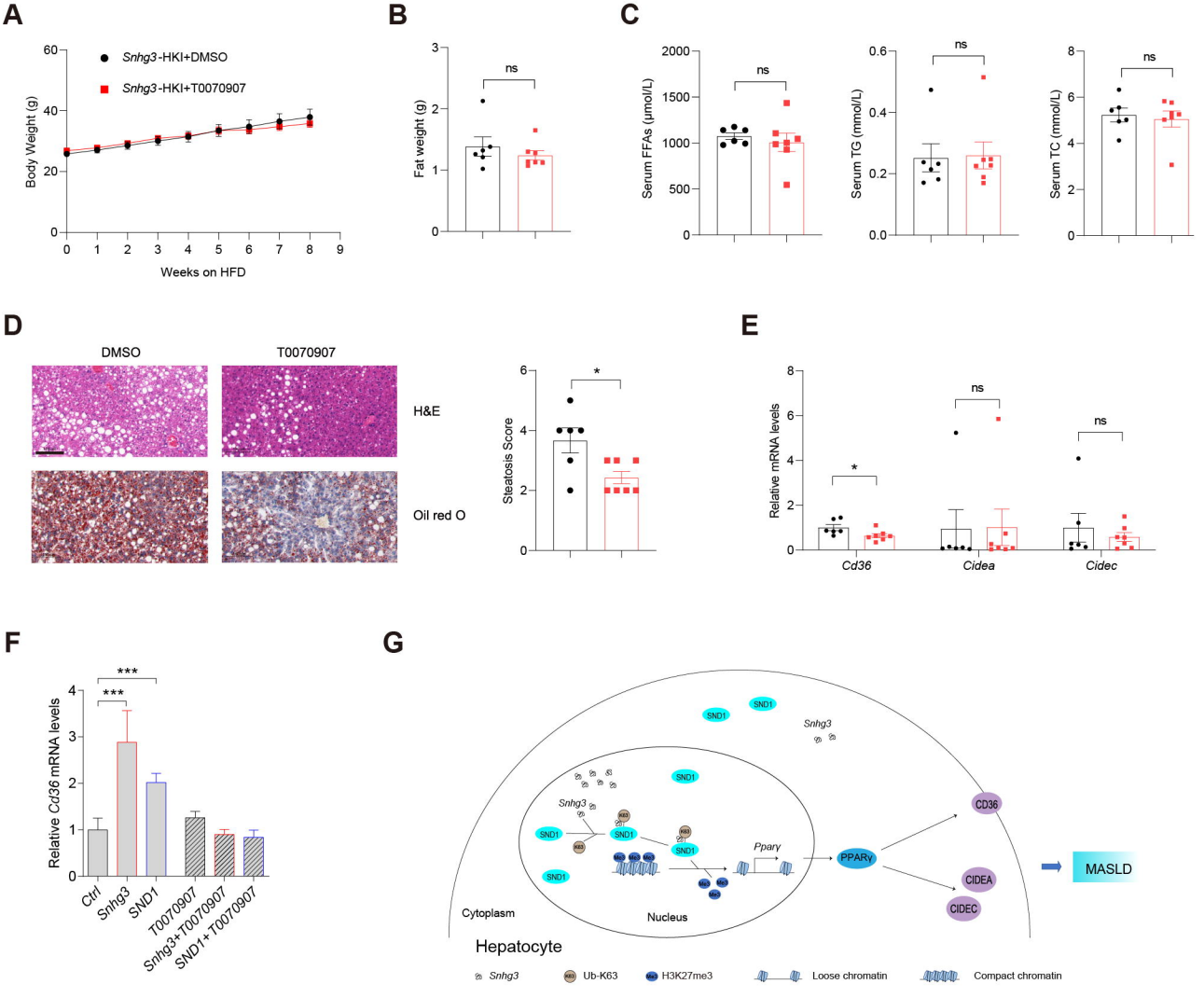
A
Snhg3-HKI+DMSO
Snhg3-HKI+T0070907
Body Weight (g)
Weeks on HFD
B
Fat weight (g)
ns
C
Serum FFAs (μmol/L)
Serum TG (mmol/L)
Serum TC (mmol/L)
ns
D
DMSO
T0070907
H&E
Oil red O
Steatosis Score
*
E
Relative mRNA levels
Cd36
Cidea
Cidec
F
Relative Cd36 mRNA levels
***
Ctrl
Snhg3
SND1
T0070907
Snhg3+T0070907
SND1+T0070907
G
SND1
Snhg3
Ppary
PPARγ
CD36
CIDEA
CIDEC
MASLD
Cytoplasm
Nucleus
Hepatocyte
Ub-K63
H3K27me3
Loose chromatin
Compact chromatin

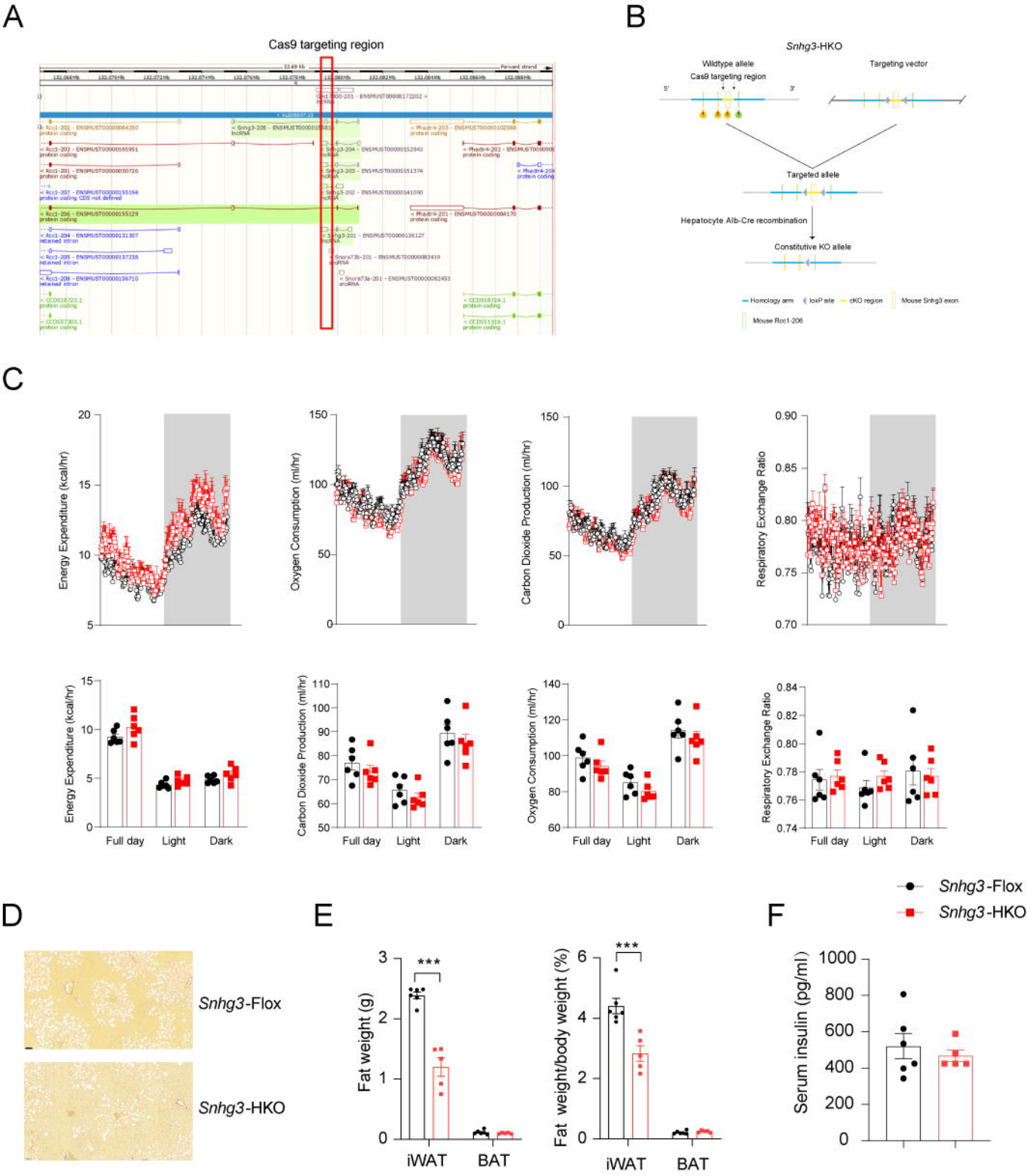
A
Cas9 targeting region
B
Snhg3-HKO
Wildtype allele
Cas9 targeting region
Targeting vector
Targeted allele
Hepatocyte Alb-Cre recombination
Constitutive KO allele
Homology arm
loxP site
cKO region
Mouse Snhg3 exon
Mouse Rcc1-206
C
Energy Expenditure (kcal/hr)
Oxygen Consumption (ml/hr)
Carbon Dioxide Production (ml/hr)
Respiratory Exchange Ratio
Full day
Light
Dark
Snhg3-Flox
Snhg3-HKO
D
Snhg3-Flox
Snhg3-HKO
E
Fat weight (g)
Fat weight/body weight (%)
iWAT
BAT
***
F
Serum insulin (pg/ml)

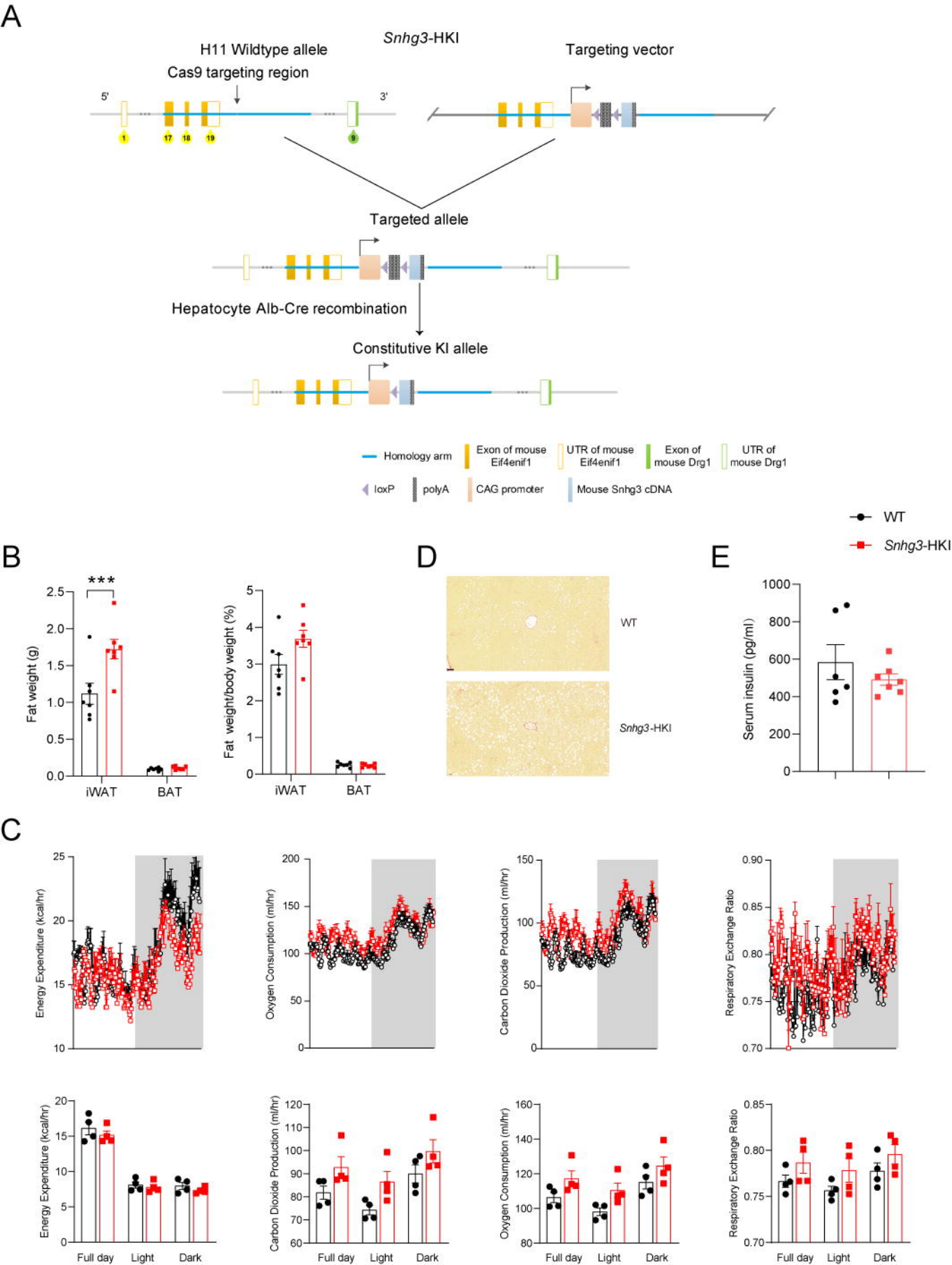
A
Snhg3-HKI
H11 Wildtype allele
Cas9 targeting region
Targeting vector
5'
3'
1
17
18
19
9
Targeted allele
Hepatocyte Alb-Cre recombination
Constitutive KI allele
Homology arm
Exon of mouse Eif4enif1
UTR of mouse Eif4enif1
Exon of mouse Drg1
UTR of mouse Drg1
loxP
polyA
CAG promoter
Mouse Snhg3 cDNA
WT
Snhg3-HKI
B
***
Fat weight (g)
iWAT
BAT
Fat weight/body weight (%)
D
WT
Snhg3-HKI
E
Serum insulin (pg/ml)
C
Energy Expenditure (kcal/hr)
Oxygen Consumption (ml/hr)
Carbon Dioxide Production (ml/hr)
Respiratory Exchange Ratio
Full day
Light
Dark

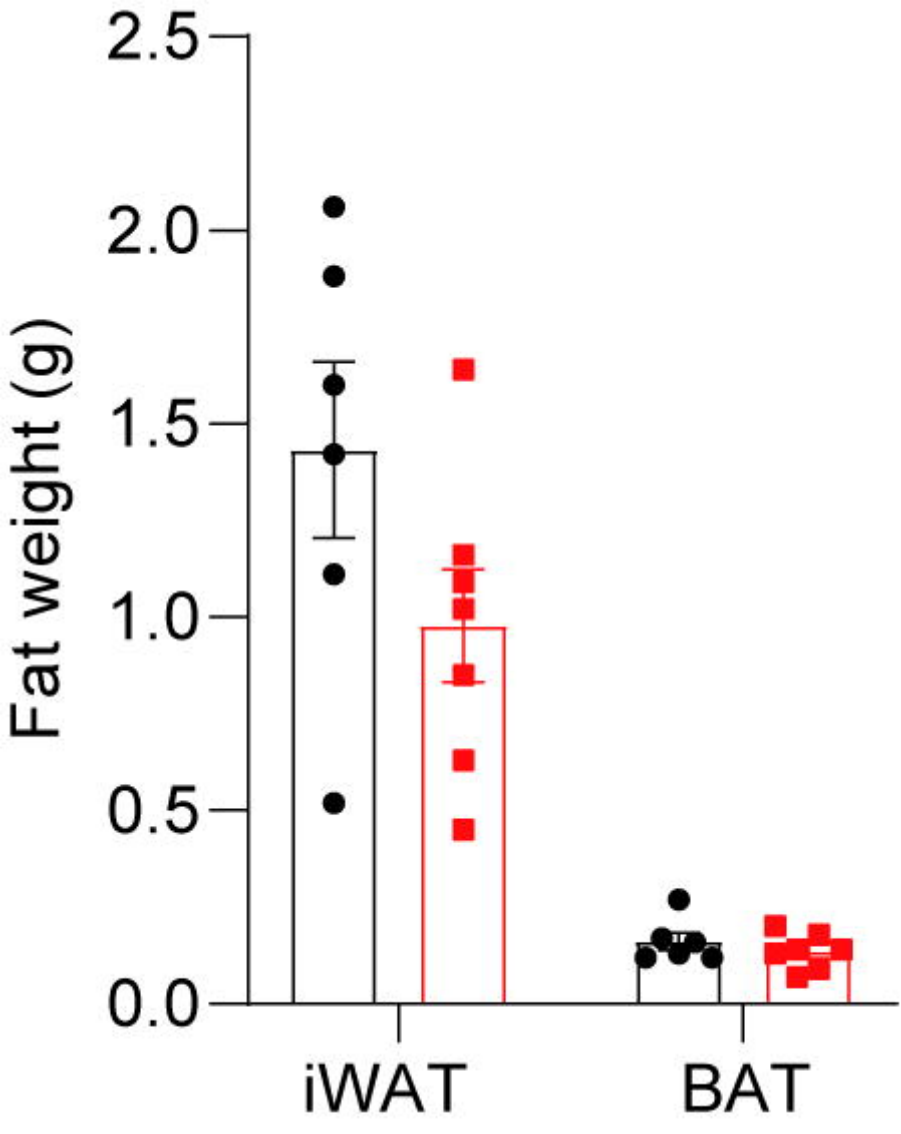
2.5
2.0
1.5
1.0
0.5
0.0
Fat weight (g)
iWAT
BAT